RSC Advances

PAPER

View Article Online
View Journal | View Issue

Cite this: *RSC Adv.*, 2023, **13**, 34756

One-pot synthesis of pyrazolo[4,3-*d*]thiazole derivatives containing α-aminophosphonate as potential Mur A inhibitors against MDR pathogens with radiosterilization and molecular modeling simulation†

Ahmed Ragab,[a] Seham A. Ibrahim,[b] Dina S. Aboul-Magd*[c] and Mohamed H. Baren[b]

The present study involves the synthesis of a new series of α-aminophosphonate derivatives in good yields with a simple workup *via* the Kabachnik–Fields reaction using lithium perchlorate ($LiClO_4$) as a catalyst to facilitate the reaction. All the newly synthesized compounds were confirmed using various physical, spectroscopic, and analytical data, and the obtained results correlated with the proposed molecular structure. The *in vitro* antimicrobial activities of each compound were evaluated against different clinical isolates. The results indicated that among these derivatives, two compounds (**5a** and **5b**) were the most active and displayed potent activity with MICs in the range from 0.06 to 0.25 μg mL^{-1} compared with fosfomycin and fluconazole as standard antibiotics. Moreover, the synthesized phosphonates displayed a broad spectrum of bactericidal and fungicidal activities depending on MICs, MBCs/MFCs, and the time-kill kinetics. In addition, the checkerboard assay showed synergistic and partial synergistic activities between the active compounds combined with fosfomycin and fluconazole. Furthermore, the SEM images showed distinct ruptures of the OM integrity of the FOS-R *E. coli* at their MICs, which was further indicated by the increased EtBr accumulation within the bacterial cells. Moreover, active derivatives revealed MurA inhibitory activity with IC_{50} values of 3.8 ± 0.39 and 4.5 ± 0.23 μM compared with fosfomycin (IC_{50} = 12.7 ± 0.27 μM). To our surprise, exposing **5a** and **5b** compounds to different gamma radiation doses revealed that 7.0 kGy eradicated the microbial load completely. Finally, the results of quantum chemical study supported the binding mode obtained from the docking study performed inside the active site of MurA (**PDB**: 1UAE), suggesting that these phosphonates may be promising safe candidates for MDR infection therapy clinical trials with no toxic effects on the normal human cells.

Received 16th October 2023
Accepted 14th November 2023

DOI: 10.1039/d3ra07040a

rsc.li/rsc-advances

1. Introduction

Antibiotic resistance is one of the biggest threats to the global healthcare system, according to the World Health Organization.[1] The α-aminophosphonates (AAPs) are an important class of organophosphorus compounds with structural amino acid analogs where a carboxylic group is substituted by phosphonic acid or related groups.[2] As a result of their remarkable biological and physical properties and their value as synthesis intermediates, AAPs have been used in various fields, including manufacturing, agriculture, and medicine. They are discovered to be antibacterial,[3] anti-Alzheimer,[4] antiviral,[5] anti-inflammatory,[6] anti-HIV,[7] antitumor,[8] anti-proliferative and apoptosis-inducing,[9] herbicidal,[10] and insecticidal[11] agents. Additionally, the phosphonates and α-aminophosphonates make up an intriguing class of substances that have been used to synthesize fire retardants,[12–14] dispersants, corrosion inhibitors,[15,16] dental additives,[17,18] and deposition prevention agents.[19]

Numerous methods have been developed for synthesizing phosphonates and α-aminophosphonates due to the many applications.[20,21] Many drugs containing phosphorus are released as drugs or prodrugs in order to achieve higher selectivity and bioavailability.[22] For example, clindamycin phosphate I (broad-spectrum antibiotic),[23] tedizolid phosphate antibiotic II (inhibits bacterial protein synthesis),[24] fosfluconazole III (anti-fungal agent),[25] dexamethasone phosphate IV and prednisolone phosphate V (anti-inflammatory agents),[26] etoposide phosphate

[a]*Chemistry Department, Faculty of Science (Boys), Al-Azhar University, Nasr City, Cairo 11884, Egypt. E-mail: ahmed_ragab7@ymail.com; ahmed_ragab@azhar.edu.eg*
[b]*Chemistry Department, Faculty of Science, Tanta University, Tanta 31527, Egypt. E-mail: seham.ibrahim@science.tanta.edu.eg; sehamabdelatif@yahoo.com*
[c]*Drug Radiation Research Department, National Center for Radiation Research and Technology (NCRRT), Egyptian Atomic Energy Authority, Egypt. E-mail: dina.a.a.soliman@gmail.com*

† Electronic supplementary information (ESI) available. See DOI: https://doi.org/10.1039/d3ra07040a

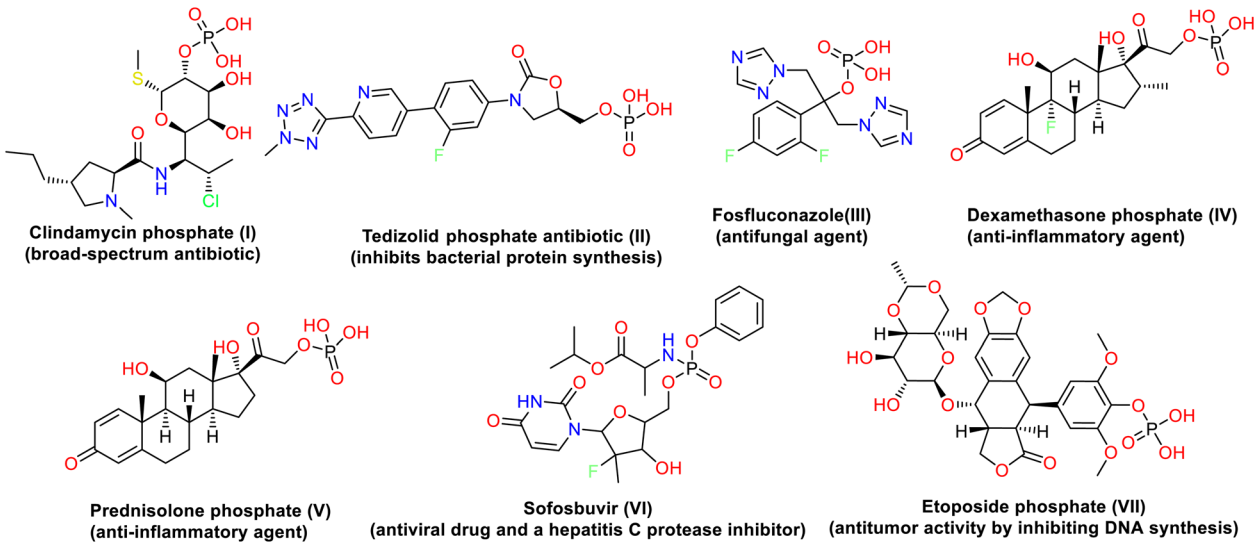

Fig. 1 Drugs containing a phosphonate group and their biological target.

VI (has antitumor activity by inhibiting DNA synthesis),[27] and sofosbuvir VII (antiviral drug and a hepatitis C protease inhibitor)[28] (Fig. 1). Moreover, the presence of heterocyclic moieties in the structure of α-aminophosphonates appears to have substantially impacted biological activities. Additionally, introducing these heterocyclic rings, such as quinazoline, pyrazole, thiazole, pyridine, and chromene, in the structure is particularly helpful in enhancing their activity.[29] For that reason, the synthesis of α-aminophosphonates has attracted considerable attention, and significant progress has been made in developing more efficient methods for the synthesis of these compounds.[30] Two main pathways have been developed for the synthesis of α-aminophosphonates: the Pudovik and Kabachnik–Fields reactions. The Kabachnik–Fields reaction involved the nucleophilic addition of an amine to a carbonyl compound followed by the addition of a dialkyl or diaryl phosphite to the resulting imine in either one-step or multi-step operation using Lewis acids as catalysts.[31,32] The Kabachnik–Fields reaction still gains interest due to the challenging synthetic procedures and the potential biological activity of the resulting α-aminophosphonic derivatives.[33]

As a result, novel synthesis has been established for the management of thiazolyl-pyrazole derivatives, allowing for their chemical diversity, preferred biological efficacy, and low toxicity for medical purposes. Various thiazolyl-pyrazole analogues have been synthesized and investigated for biological activity as cyclooxygenase inhibitors, antioxidants, analgesics, and anti-inflammatory drugs, as well as their potential as antibacterial, antifungal, antioxidant, and anticancer agents.[34–37] Targeting the biosynthetic steps in the bacterial cell wall assembly is a promising way to produce new antibacterial agents, as many clinically important antibiotics such as penicillins and vancomycin demonstrate.[38] MurA is important in the first cytoplasmic step of peptidoglycan biosynthesis. It is a UDP-*N*-acetylglucosamine enolpyruvyl transferase that catalyzes the transfer of enolpyruvate from phosphoenolpyruvate (PEP) to the 30-hydroxy group of uridine diphospho-*N*-acetylglucosamine (UNAG).[39] This transfer originated by binding UNAG to the enzyme's active site, followed by the binding of PEP. Cys115 and Asp305 are two amino acids that are essential in forming this product, particularly for the deprotonation of the C3 atom of the tetrahedral intermediate and for the final product release.[40] MurA is a validated antibacterial drug discovery target. It represents selective targeting because it is only present in bacteria and is neither required nor present in human cells.[40] Sterilization of pharmaceutics is required to be safely and effectively used. It is a unique critical procedure. The anonymous "sterilization" is defined as the use of a suitably designed, validated and controlled process to inactivate or reduce the viable microorganisms, determined by the sterility assurance level (SAL) < 10^{-6}, within the target product.[41] One of the most widely used methods is gamma radiation *via* a source of radiation such as Cobalt-60 (^{60}Co). The use of gamma radiation has many advantages such as easy penetration into the product, ensuring sterility and effectiveness independent of temperature and pressure.[42,43]

Based on the previous data and in continuation of our works aiming to synthesize heterocyclic molecules with remarkable biological activities,[44–47] we aimed to investigate the use of $LiClO_4$ as a catalyst to synthesize novel thiazolyl-pyrazole heterocycle-containing α-aminophosphonate derivatives *via* a "one-pot" three-component reaction as excellent non-cytotoxic alternatives for synthesizing α-aminophosphonates. Moreover, the newly designed derivatives were evaluated for their antimicrobial activity (*i.e.*, MIC, MBC/MFC, time-killing kinetics, and drug combination studies) against MDR microbial isolates. The effects of phosphonates on the outer membrane of *E. coli* were studied using SEM analysis and ethidium bromide (EtBr) dye accumulation assay. The evaluation of MurA inhibition activity as a mode of action was confirmed by molecular docking and quantum chemical studies.

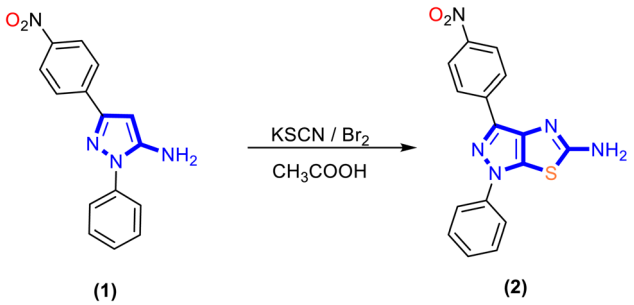

Scheme 1 Synthesis of new 1*H*-pyrazolo[4,3-*d*]thiazol-5-amine derivative **2**.

2. Result and discussion

2.1. Chemistry

In the present work, a new series of α-aminophosphonate derivatives **3**, **4**, **5a**, **5b**, **6a** and **6b** were synthesized in good yields by a one-pot three-component reaction of 5-amino-pyrazolethiazole, aldehyde derivatives, and diethyl and/or diphenyl phosphite at room temperature in the presence of lithium perchlorate ($LiClO_4$) as a catalyst *via* the Kabachnik–Fields reaction (Schemes 2 and 3).

First, 5-amino-1*H*-pyrazolo[4,3-*d*]thiazole derivative **2** was prepared by the reaction of 5-amino pyrazole derivative **1** with bromine and potassium thiocyanate as described previously[48] (Scheme 1). Then, a molar ratio (1 : 1 : 1) of 5-amino-1*H*-pyrazolo [4,3-*d*]thiazole derivative **2**, trialkyl phosphite, and appropriate aldehyde in dichloromethane (CH_2Cl_2) was stirred at room temperature for 48 h in the presence of anhydrase lithium perchlorate ($LiClO_4$) as the one-pot three-component reaction, and the progress of the reaction was monitored by TLC until the reaction was complete, as described in Schemes 2 and 3. The mechanism for synthesizing α-aminophosphonates using $LiClO_4$ as a catalyst is illustrated in Scheme S1.† First, the reaction started by activating the carbonyl group of aldehydes with the Lewis acid catalyst ($LiClO_4$), followed by the condensation of the carbonyl group attached with primary amines to afford the Schiff base. Then the nitrogen of the Schiff base that is formed in the first step donated a pair of electrons to make a coordinate bond with $LiClO_4$. This coordination makes nitrogen positively charged and therefore induces a partial positive charge on sp^2 carbon. In addition, the free pair of electrons of phosphorus attack the partially positively charged carbon, followed by the elimination of phenol or ethanol, and afford cyclic α-aminophosphonates.

The chemical structures of α-aminophosphonate derivatives **3**, **4**, **5a**, **5b**, **6a** and **6b** were characterized by IR, ^{1}H NMR, ^{13}C NMR, mass spectroscopy and elemental analyses, and their data are presented in the experimental section. The IR spectra of compounds **3**, **4**, **5a**, **5b**, **6a** and **6b** showed the NH band in the range of 3320–3378 cm^{-1}. The sharp band observed in the range of 1237–1277 cm^{-1} is attributed to P=O, and a band for P–C stretching occurred in the range of 769–779 cm^{-1}. The ^{1}H NMR spectra of the synthesized derivatives exhibited a characteristic signal at δ 9.29–9.72 ppm assigned to the –NH group and a signal in the range δ 5.97–7.64 ppm as a singlet signal assigned to P–CH of all the title compounds. Moreover, for diethyl phosphonate derivatives **3** and **4**, the methylene and methyl protons of P–O–CH_2CH_3 displayed as a quartet at δ 3.85 ppm and triplet at δ 1.05–1.19 ppm. The ^{13}C NMR spectra of diethyl phosphonate derivatives **3** and **4** revealed chemical shifts for methylene and methyl carbons observed at δ 66.80–66.81 ppm and δ 12.23–22.05 ppm, respectively. Moreover, the chemical shift for P–CH carbons was observed at δ 59.58–66.84 ppm. The compounds were analyzed by mass spectroscopy, and M^+ ions were observed in the expected *m*/*z* values.

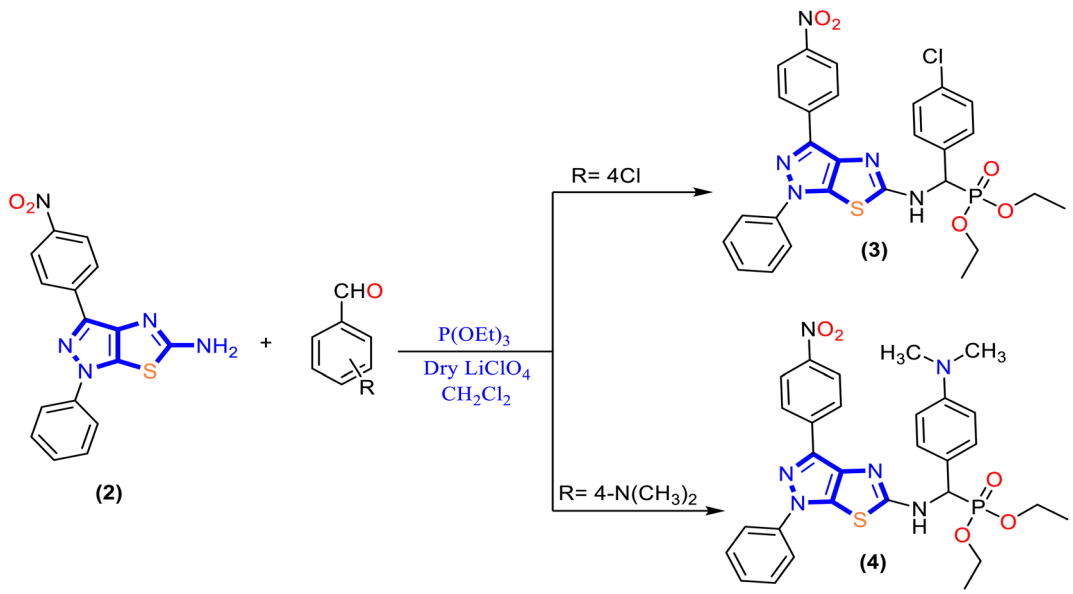

Scheme 2 Synthetic route for novel ethyl α-aminophosphonates **3** and **4**.

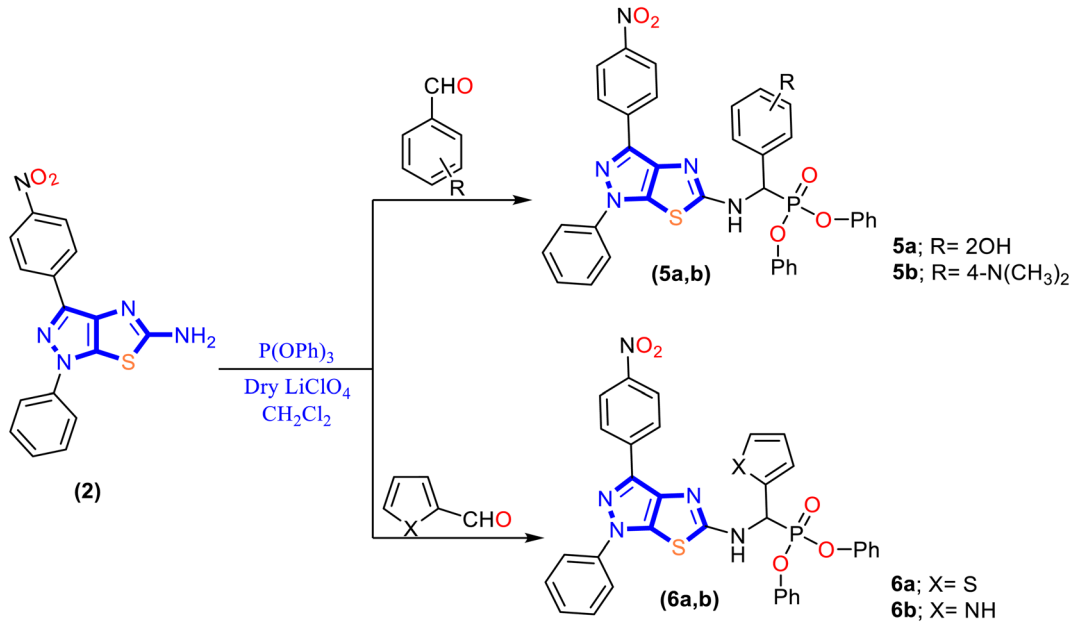

Scheme 3 Synthetic route for novel α-aminophosphonates **5a**, **5b**, **6a** and **6b**.

2.2. Biological evaluation

2.2.1. Antimicrobial screening. To examine the inhibitory effect of different phosphonate compounds on the MDR bacterial and fungal isolates, the inhibition was measured in plates *via* the formation of growth inhibition halos on the microbial lawns (Table 1). The test compounds and reference drugs were used initially at a concentration of 10 μM (DMSO), and the results are recorded in Table 1. All the tested phosphonates exhibited significant antimicrobial activity. The measurement of the inhibition zones of each compound showed that **5a** and **5b** were the most active compounds, which inhibited the growth of both bacterial and fungal isolates with ZOI ranging from 21 mm to 25 mm, as shown in Fig. 2. In the case of fosfomycin, the bacterial isolates showed variable resistance profiles that differ from sensitivity (ZOI = 17–19 mm) to resistance as in the case of *E. coli* (ZOI = 11 mm). In addition, fluconazole as a positive control for antifungal activity showed an intermediate response to the fungal isolates with a zone of inhibition of 17 mm.

2.2.2. MICs, MBC, and MFC. The MIC, MBC, and/or MFC were determined for the synthesized α-aminophosphonate derivatives **2–6** and the two reference antibiotics (fosfomycin and fluconazole). The results indicated moderate to excellent

Table 1 Diameter of inhibition zones in millimetres of the newly synthesized phosphonates against different Gram +ve and Gram −ve bacteria, as well as *Candida* isolates[a]

	Average diameter of inhibition zone (ZI) in mm					
	Bacteria					
	Gram +ve		Gram −ve		Fungi	
Cpd. no.	*E. faecalis*$_{KA247}$	*S. aureus*$_{KA112}$	*E. coli*$_{KA780}$	*P. mirabilis*$_{KA320}$	*C. albicans*$_{KA205}$	*C. tropicalis*$_{KA205}$
2	17 ± 0.00	17 ± 0.39	17 ± 0.62	16 ± 0.79	17 ± 0.16	16 ± 0.63
3	18 ± 0.05	18 ± 0.31	19 ± 0.14	17 ± 0.71	17 ± 0.88	17 ± 0.48
4	16 ± 0.80	17 ± 0.00	17 ± 0.54	16 ± 0.34	16 ± 0.67	16 ± 0.54
5a*	24 ± 0.20	24 ± 0.51	25 ± 0.28	23 ± 0.44	22 ± 0.76	22 ± 0.43
5b**	23 ± 0.88	24 ± 0.03	25 ± 0.00	23 ± 0.78	22 ± 0.22	21 ± 0.32
6a	18 ± 0.74	19 ± 0.00	19 ± 0.66	18 ± 0.50	20 ± 0.89	20 ± 0.20
6b	22 ± 0.55	23 ± 0.77	24 ± 0.86	22 ± 0.12	21 ± 0.91	21 ± 0.70
FO	17 ± 0.34	18 ± 0.32	11 ± 0.23	19 ± 0.13	NA	NA
FCA	NA	NA	NA	NA	17 ± 0.99	17 ± 0.15
DMSO	−ve	−ve	−ve	−ve	−ve	−ve

[a] ±: standard error mean; each value is the mean of three values; **FO**: fosfomycin; **FCA**: fluconazole; NA: non-applicable; −ve: no growth detected; CLSI breakpoints: zone diameter for fosfomycin "M100, 30th edition, 2020" (≥16 [susceptible], 13 to 15 [intermediate], and ≤12 [resistant] mm); zone diameter for fluconazole "M27-A4, 4th edition, 2017" (≥19 [susceptible], 15 to 18 [intermediate], and ≤14 [resistant] mm).

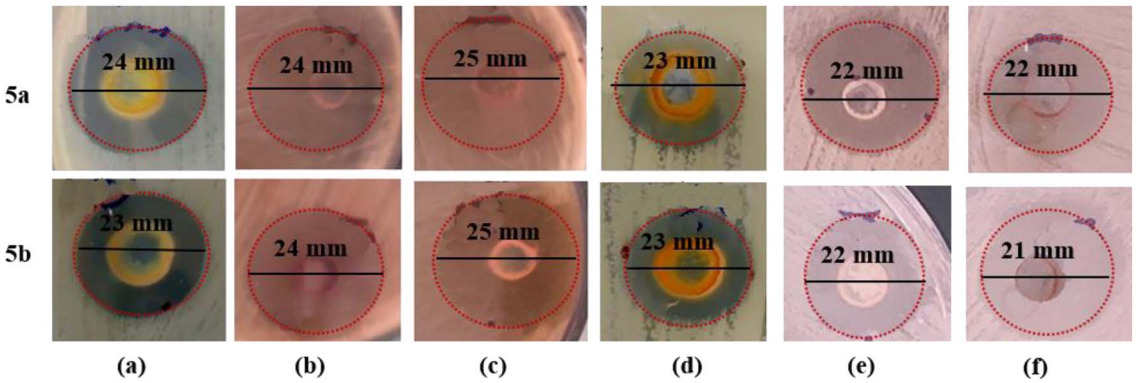

Fig. 2 Diameter of inhibition zones of the most active compounds **5a** and **5b** against (a) *E. faecalis*$_{KA247}$, (b) *S. aureus*$_{KA112}$, (c) *E. coli*$_{KA780}$, (d) *P. mirabilis*$_{KA320}$, (e) *C. albicans*$_{KA205}$, and (f) *C. tropicalis*$_{KA205}$.

activities against clinical isolates. The activity was assessed for each drug individually in the range from 0.06 μg mL^{-1} to 256 μg mL^{-1} in TSB and SB media, and the results are presented in Table 2. The data displayed that the two diphenyl α-aminophosphonates **5a** and **5b** were the most active compounds with MIC ranging from 0.06 μg mL^{-1} to 0.25 μg mL^{-1} and MBC values ranging from 0.03 to 0.125 μg mL^{-1} compared with fosfomycin MIC = 16–256 μg mL^{-1} and MBC = 32–256 μg mL^{-1} and fluconazole MIC = 2–4 μg mL^{-1} and MFC = 2 μg mL^{-1}. The remaining compounds showed MICs ranging from 0.125 μg mL^{-1} to 32 μg mL^{-1}. At the same time, the MICs for fosfomycin ranged from 8 μg mL^{-1} to 16 μg mL^{-1}, except with *E. coli* (MIC = 256 μg mL^{-1}, *i.e.*, resistant). In the case of fluconazole, *C. albicans* and *C. tropicalis* showed MIC values of 2 and 4 μg mL^{-1}, respectively.

The structure–activity relationship (SAR) exhibited that modification of 5-amino-1*H*-pyrazolo[4,3-*d*]thiazole derivative **2** with a phosphonate group enhancement antimicrobial activity in general. In addition, diphenyl α-aminophosphonate derivatives **5** and **6** demonstrated a higher activity than that of diethyl α-aminophosphonates **3** and **4**. In terms of comparison, the presence of an electron-withdrawing group as a chlorine atom in benzyl phosphonate derivative **3** showed MIC values ranging from 1 to 2 μg mL^{-1} and MBC (1–4 μg mL^{-1}) and MFC (0.5–1 μg mL^{-1}), while replacing a chlorine atom with *N*,*N*-dimethyl amine (electron donating group) at the same position as compound **4** causes a dramatic decrease in the activity on both bacterial and fungal isolates, but still promising than fosfomycin (except in case of *E. faecalis*$_{KA247}$) and fluconazole with MIC values of 8–16 μg mL^{-1}, MBC of 8–16 μg mL^{-1} and MFC of 1–2 μg mL^{-1}, and these results indicate that the presence of an electron-withdrawing group in the para position to benzyl phosphonate is desirable. Interestingly, replacing diethyl groups in compound **4** with diphenyl groups that appeared in compound **5b** improved the antimicrobial activity with 64–133 folds against bacterial isolates and 4–16 folds against fungal isolates based on MIC values.

Table 2 MIC, MBC and MFC of the phosphonate compounds against the panel of MDR bacterial and fungal isolates expressed in μg mL^{-1}[a]

	MIC (mean ± SEM) (μg mL^{-1}) (MBC/MIC or MFC/MIC)					
	Bacteria					
	Gram +ve		Gram −ve		Fungi	
Cpd. no.	*E. faecalis*$_{KA247}$	*S. aureus*$_{KA112}$	*E. coli*$_{KA780}$	*P. mirabilis*$_{KA320}$	*C. albicans*$_{KA205}$	*C. tropicalis*$_{KA205}$
2	8 (1)	8 (0.5)	4 (0.5)	8 (1)	1 (0.5)	1 (2)
3	2 (2)	1 (2)	1 (1)	2 (1)	1 (1)	1 (0.5)
4	16 (1)	8 (2)	8 (1)	16 (1)	2 (0.5)	2 (1)
5a*	0.125 (0.5)	0.06 (0.5)	0.06 (0.5)	0.125 (0.5)	0.125 (0.5)	0.125 (1)
5b**	0.125 (1)	0.06 (1)	0.06 (0.5)	0.25 (0.5)	0.125 (1)	0.5 (0.5)
6a	2 (0.5)	1 (1)	1 (0.5)	2 (1)	0.5 (0.5)	0.5 (1)
6b***	0.25 (0.5)	0.125 (0.5)	0.125 (0.5)	0.25 (1)	0.25 (1)	0.5 (1)
FO	8 (1)	8 (0.4)	256 (1)	16 (1)	NA	NA
FCA	NA	NA	NA	NA	2 (1)	4 (0.5)
DMSO	−ve	−ve	−ve	−ve	−ve	−ve

[a] ±: standard error mean; each value is the mean of three values; **FO**: fosfomycin; **FCA**: fluconazole; NA: non-applicable; −ve: no growth detected; CLSI breakpoints: MIC breakpoints (M100, 30th edition, 2020) for fosfomycin (≤64 [susceptible], 128 [intermediate], and ≥256 [resistant] μg mL^{-1}); MIC breakpoints for fluconazole (M27-A4, 4th edition, 2017): (≤2 [susceptible], 4 [intermediate], and ≥8 [resistant] μg mL^{-1}).

Furthermore, grafting the hydroxyl group in the ortho position to benzyl phosphonate in compound **5a** showed enhancement in the inhibitory activity against *P. mirabilis*$_{KA320}$ (MIC = 0.125 μg mL^{-1}) compared to *N*,*N*-dimethyl amine in the para position as compound **5b** (MIC = 0.25 μg mL^{-1}) and increased the minimal bactericidal (MBC) and fungicidal (MFC) activity to a two-fold value against *E. faecalis*$_{KA247}$ and *S. aureus*$_{KA112}$ and that may be related to increasing the electron density that occurs by a hydroxyl group in the ortho position rather than a para position to *N*,*N*-dimethyl amine. In addition, replacing aromatic phenyl in methyl phosphonate with heterocyclic rings as thiophene core **6a** and pyrrole core **6b** exhibited good antimicrobial activity, but less than the benzyl phosphonate group. In addition, the presence of the NH group in pyrrole revealed a higher activity with MIC values of 0.125–0.25 μg mL^{-1} against bacteria (~8 folds) and 0.25–0.50 μg mL^{-1} (~1–2 folds) against fungal isolates, and this activity may be related to sulfur that has higher electronegativity and, therefore, a lesser tendency to donate its lone pair.

Moreover, it has been exploited that MBC/MFC is the lowest concentration of antibiotic to kill a certain bacterium/fungus. It involves adding extra steps performed after the determination of MIC. The antimicrobial agents are considered bactericidal/fungicidal if the MBC or MFC ratio is not greater than four times the MIC. The tested phosphonate compounds showed bactericidal and fungicidal effects. In addition, both fosfomycin and fluconazole showed bactericidal and fungicidal activities against different isolates.

2.2.3. Effect of phosphonates on time-kill curves. The time-kill kinetics were used to monitor the growth of MDR microbial isolates and to observe the changes in the bacterial cell counts after treatment of the most active phosphonate derivatives **5a**, **5b**, and positive controls (fosfomycin and fluconazole) during certain time intervals at 1/2MIC and MIC. As shown in Fig. 3, the time-kill profiles of **5a** and **5b** displayed ≥3log10 microbial reduction relative to the initial inoculum with the reference antibiotics, indicating bactericidal and fungicidal activities against all the pathogenic isolates. The bacterial cell counts (control) incubated with fosfomycin at MIC only showed complete bacterial growth reduction upon incubation for 12 h and 16 h. Except in the case of FOS-R *E. coli* isolates, a reduction in the bacterial cell counts has been observed at the selected time intervals till 12 h cultivation, followed by an increase in the cell counts after 18 h. Moreover, the fungal isolates showed maximum reduction in the cell counts upon treatment with fluconazole after 48 h. These findings were consistent with the resistance profile of the different bacterial and fungal isolates tested. On the contrary, Fig. 3 shows the maximum killing rate upon exposure to phosphonate compounds **5a** and **5b** after 6 h and 8 h; and after 16 h and 18 h, respectively, with the bacterial and fungal isolates. At 1/2MIC, the bacterial and fungal isolates showed a reduction in the viable cell counts after exposure to phosphonates after 24 h and 72 h, respectively.

2.2.4. Synergy testing by checkerboard microdilution. The overuse of antibiotics increases the emergence rate of resistance of pathogens to different antibiotics.[49,50] Accordingly, the combination therapy of clinically used antibiotics with other antimicrobial agents has been used extensively to reduce the rate of resistance amongst microorganisms.[51,52] The checkerboard microdilution assay assessed the combination of the most potent phosphonate compounds **5a** and **5b** with fosfomycin and fluconazole to act as an add-on to induce a reduction in their MICs against the different bacterial and fungal isolates tested.

The synergistic activity was determined according to the fractional inhibitory concentration index (ΣFICI), in which the value of ΣFICI ≤ 0.5 indicates synergism between the compound and the antibiotic. Indeed, as shown in Table 3, both phosphonate compounds **5a** and **5b** exhibited ΣFICI ≤ 0.5 and from 0.5 < FICI > 1 in the drug combinations reported (*i.e.*, able to re-sensitize the isolates to antibiotics), suggesting synergistic and partial synergistic antimicrobial activities. Finally, these phosphonate derivatives **5a** and **5b** considerably reduced the MIC of fosfomycin and fluconazole against all the tested clinical isolates.

2.2.5. Effects of phosphonates on the *E. coli* outer membrane (OM) structure. Our work was extended to study the SEM analysis employed to investigate the surface microanatomy and cellular interior. The antibacterial effect is thought to be related to interactions between the cell membrane of the microorganism and biocides.[53,54] The fosfomycin-resistant (FO-R) *E. coli*$_{KA780}$ isolate was selected to determine the effect of active phosphonates **5a** and **5b** on the bacterial outer membrane integrity. The OM barrier presents bacteria with highly selective permeability, thereby forbidding the clinical use of various antibiotics. As described in (Fig. 4), the SEM image revealed perturbation in the membrane and distinct ruptures of the OM integrity on the treatment of the most active phosphonate derivatives **5a** and **5b** with *E. coli* compared with untreated DMSO.

2.2.6. Fluorescent dye accumulation reduced by phosphonates. To evaluate the substrates' amounts accumulated on the outer membrane (OM) integrity of *E. coli*, the ethidium bromide (EtBr) dye accumulation assay was used. The amount of EtBr dye accumulation implies the substrate efflux level by the detected cells expressing the drug transporters. The EtBr showed strong fluorescence upon binding with the DNA and/or in a hydrophobic environment.[55] In this assay, EtBr was used to monitor the substrate accumulation in *E. coli* Kam3-AcrB, and the resistance-nodulation-division pump modulation (PAβN) was also used as a positive control.[56]

As shown in Fig. 5, adding PAβN increases the accumulation of EtBr in the *E. coli* strain. Similarly, the addition of phosphonates showed an increase in the accumulation of EtBr at their different MIC levels. Finally, it can be concluded that the phosphonate treatment caused a dose-dependent increase in the EtBr uptake, indicating evidence of the dramatic effect of phosphonates on the integrity of the outer membrane (OM) integrity.

2.2.7. *In vitro* cytotoxic activity on normal cell lines. In order to evaluate the safety of the phosphonate compounds, the cytotoxicity of most two active compounds **5a** and **5b** was evaluated *in vitro* against two non-cancerous cell lines (BNL and Vero). The findings of the cytotoxic activity were recorded in

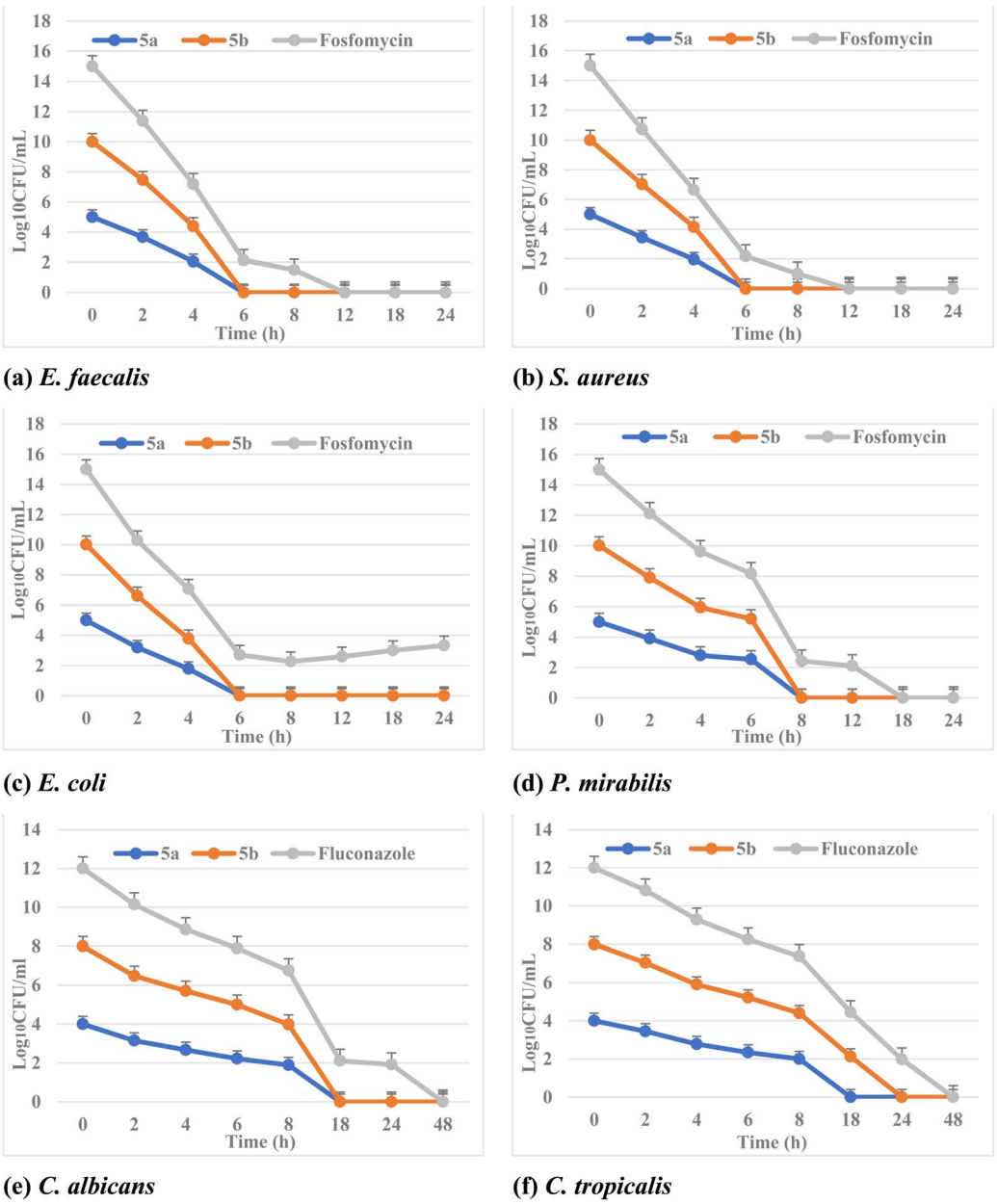

Fig. 3 Time-kill curve of different MDR bacterial and fungal isolates (a) *E. faecalis*$_{KA247}$, (b) *S. aureus*$_{KA112}$, (c) *E. coli*$_{KA780}$, (d) *P. mirabilis*$_{KA320}$, (e) *C. albicans*$_{KA205}$ and (f) *C. tropicalis*$_{KA205}$ with **5a**, **5b**, fosfomycin and fluconazole at the concentration of MIC.

Table 3 Combinations effects of compounds **5a** and **5b** with antibiotics fosfomycin and fluconazole against the different clinical isolates

	Fractional inhibitory concentration index (ΣFICI)/effect					
	Bacteria[a]					
	Gram +ve		Gram −ve		Fungi[b]	
Cpd. no.	*E. faecalis*$_{KA247}$	*S. aureus*$_{KA112}$	*E. coli*$_{KA780}$	*P. mirabilis*$_{KA320}$	*C. albicans*$_{KA205}$	*C. tropicalis*$_{KA205}$
5a*	0.5/S	0.25/S	0.25/S	0.5/S	0.75	0.5/S
5b**	0.5/S	0.5/S	0.25/S	0.25/S	0.75/P	0.75/P

[a] Combination of **5a** or **5b** with fosfomycin. [b] Combination of **5a** or **5b** with fluconazole; FICI ≤ 0.5 (synergism); 0.5 < FICI > 1 (partial synergism); 1 ≤ FICI < 2 (indifference); FICI ≥ 2 (antagonism).

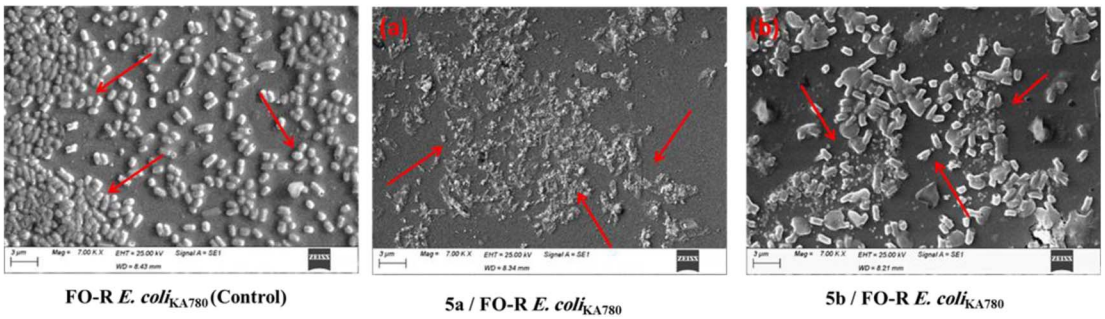

Fig. 4 Microscopic observation of the morphological alterations of fosfomycin-resistant *E. coli*$_{KA780}$ treated with DMSO (1%) and with phosphonate compounds (a) **5a** and (b) **5b** for 12 h using a scanning electron microscope (SEM).

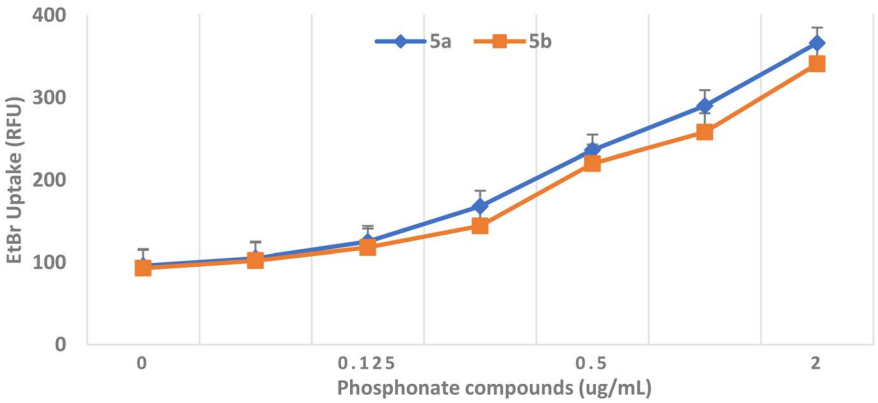

Fig. 5 EtBr accumulation in *E. coli* Kam3-AcrB. *E. coli* was treated with phosphonate compounds **5a** and **5b** at a concentration ranging from 0.06 μg mL^{-1} to 2 μg mL^{-1} or DMSO (0.1%) for 12 h, followed by the addition of EtBr to give a final conc. of 4 μg mL^{-1} and RFU was determined.

Table 4. To our delight, the two compounds were found to be non-cytotoxic with IC_{50} values > 100 μM to the two cell lines compared to control (Doxorubicin). The most active compounds **5a** and **5b** in addition to DOX showed IC_{50} values of > 100, >100 and 14.7 μM with BNL and of >100, >100 and 0.68 μM with Vero. Moreover, the viability percentage of the two active compounds compared with the control drug (DOX) was also determined. The most active compound **5a** revealed non-cytotoxic activity with viability % ranged from 101.9 ± 0.58 to 94.35 ± 0.86 and from 100.2 ± 0.82 to 81.13 ± 2.6 against BNL and Vero cell lines, respectively. Moreover, the compound **5b** showed cytotoxicity against the two cell lines with viability % ranged from 99.84 ± 0.6 to 73.02 ± 1.54 in case of BNL and from 99.72 ± 2.16 to 94.5 ± 2.23 in case of Vero. In the case of the control drug, DOX showed cytotoxicity effect against BNL cell line with viability % (99.26 ± 0.9 to 7.09 ± 0.38) and against Vero cell line with viability % (101 ± 2.28 to 1.34 ± 0.18).

2.2.8. MurA enzyme inhibition assay. The most active α-aminophosphonate derivatives **5a** and **5b** were evaluated for their interfering properties on the MurA enzyme. Fosfomycin was used as a positive control. In the first step, the residual activity (RA) of MurA was determined in the presence of each compound. When the compounds were tested against MurA from *E. coli* without pre-incubation, the compounds (**5a**, **5b**, and

Table 4 *In vitro* cytotoxicity (IC_{50} in μM and viability %) of active compounds **5a** and **5b** against normal cell lines (Vero and BNL) compared with Doxorubicin[a]

	BNL		Vero	
Tested compound	IC_{50}	Viability %	IC_{50}	Viability %
5a	>100	101.9 ± 0.58 to 94.35 ± 0.86	>100	100.2 ± 0.82 to 81.13 ± 2.6
5b	>100	99.84 ± 0.6 to 73.02 ± 1.54	>100	99.72 ± 2.16 to 94.5 ± 2.23
DOX	14.7	99.26 ± 0.9 to 7.09 ± 0.38	0.68	101 ± 2.28 to 1.34 ± 0.18

[a] S.D.: standard deviation, each value is the mean of three values; BNL: mouse normal liver cells; and Vero: green monkey kidney.

Table 5 Inhibitory effects of compounds **5a**, **5b** and control antibiotics, fosfomycin (FO) on *E. coli* MurA enzyme

Compound no.	RA[a,b] % (IC_{50} in μM)	RA[a,c] % (IC_{50} in μM)
5a	32 ± 0.44 (41 ± 0.25)	0 (3.8 ± 0.39)
5b	39 ± 0.61 (45 ± 0.78)	4 ± 0.55 (4.5 ± 0.23)
FO	52 ± 0.55 (52 ± 0.33)	10 ± 0.92 (12.7 ± 0.27)

[a] RA: residual activity determined at 100 μM. [b] Time of preincubation at 0 min. [c] Time of incubation at 10 min.

fosfomycin) showed RA values less than 60%. On the contrary, when the enzymes were preincubated with compounds **5a** and **5b**, they showed RA values of 0% and 4%, respectively, as shown in Table 5. However, the fosfomycin showed RA = 10%, according to these findings. In addition, the half-inhibitory concentration (IC_{50}) values of tested derivatives were determined.

As given in Table 5, compound **5a** displayed significant inhibition of MurA enzyme from *E. coli*, with RAs of 0% and IC_{50} = 3.8 μM. Compound **5b** displayed a RA value of 7% with IC_{50} corresponding to 4.5 μM. These findings suggested the significant inhibition of MurA derived from *E. coli* displaying IC_{50} < 5 μM. Fosfomycin (FO) showed an IC_{50} value of 12.7 μM. However, these results are in accordance with the ability of these molecules to inhibit the development of FOS-R *E. coli* cells tested in this study, as was evidenced by the MIC values and time-kill kinetics. The inhibitory activity of phosphonate compounds might be attributed to the ability of active phosphonates to affect the bacterial OM integrity and, therefore, allow the penetration of phosphonates into the bacterial cell, as shown in Fig. 4.

2.2.9. Effect of gamma radiation on the microbial load of active phosphonates. The two active phosphonate compounds **5a** and **5b** were selected and exposed to a range of gamma radiation doses starting from 3.0 kGy to 20.0 kGy. After the irradiation process, the compounds were examined for any physical changes (odor, color, clarity, solubility, and form), and no changes occurred in all samples irradiated. Moreover, the chemical assay results confirmed the stability of the chemical structure of both compounds as determined using a UV-VIS spectrophotometer. In Table 6, the results indicated that the irradiation of 7.0 kGy was enough to induce a complete eradication of the microbial load.

Table 6 Microbial counts (CFU g^{-1}) of both non-irradiated and irradiated phosphonate compounds **5a** and **5b** at different gamma radiation doses

	Total count (CFU g^{-1})			
	5a		**5b**	
Dose (kGy)	Bacteria	Fungi	Bacteria	Fungi
Control (non-irradiated)	3×10^3	2×10^1	2×10^3	3×10^1
3.0	3×10^1	1×10^3	2×10^1	1×10^2
5.0	0	0	1×10^1	0
7.0	0	0	0	0
10.0	0	0	0	0
15.0	0	0	0	0
20.0	0	0	0	0

2.3. Computational studies

2.3.1. *In silico* molecular docking simulation. A docking study was conducted to identify possible binding mechanisms for the most active derivatives and to confirm the experimental data. The molecular binding to the active site of UDP-*N*-acetylglucosamine enolpyruvyl transferase (MUR A, **PDB**: 1UAE) that is isolated from *E. coli* is shown with a resolution of 1.80 Å and present in the complex with a co-crystallized ligand uridine-diphosphate-*N*-acetylglucosamine (UD1). The 3D crystal structure has been retrieved from the protein data bank (**https://www.rcsb.org/structure/1uae**). Accessed on 21/3/2023).[57] The docking simulation was achieved using Molecular Operating Environmental (MOE) 10.2009.

The docking results indicated that the most active phosphonate derivatives **5a** and **5b** revealed binding energy S = −23.46 and −20.11 kcal mol^{-1} with good binding with specified receptor targets compared with fosfomycin, S = −10.89 kcal mol^{-1}. The most active phosphonate derivatives **5a** showed one hydrogen bond backbone acceptor between the residue Val163 and oxygen of the phosphonate group with a bond length of 1.94 Å and a strength of 17%. In addition, the hydrogen atom of the hydroxyl group attached to the ortho position in benzylidene phosphonate could form a hydrogen bond sidechain acceptor with Ser162 amino acid in the receptor target. Moreover, the diphenyl α-aminophosphonate derivatives **5a** formed two arene–cation interactions between Arg91 and Arg120 with phenyl of benzylidene and phenyl phosphonate, respectively Fig. 6a. In addition, a hydrophobic interaction was observed between the phenyl group at N1 of pyrazole and phenyl of 4-nitrophenyl at C3 of pyrazole, as well as phenyl of phenyl phosphonate and appeared as blue background in the 2D structure.

Furthermore, the α-aminophosphonate derivatives **5b** exhibited binding energy S = −20.11 kcal mol^{-1} through a one arene–cation interaction between Arg120 and the phenyl group of 4-nitrophenyl at C3 of pyrazole, in addition to a great number of hydrophobic interactions Fig. 6b. The fosfomycin as a positive control demonstrated the lowest binding energy S = −10.89 kcal mol^{-1} through two hydrogen bonds from the sidechain (Arg91 and Ser162) and one hydrogen bond from the backbone (Val163). The oxygen of phosphonate in fosfomycin formed two hydrogen bond sidechains with residues Arg91 and Ser162 with a bond length of 1.97 Å (39%) and 3.24 Å (21%). In addition, the residue Val163 was bound to the oxygen of ethylene oxide through hydrogen bond backbone acceptors with a bond length of 2.06 Å and strength of 28% (all docking figures are displayed in full size in ESI† file).

2.3.2. Quantum chemical studies. Molecular orbitals dominate interactions among molecules in the term frontier molecular orbital model (FMOs). A molecule's ability to donate electrons is represented by E_{HOMO}, whereas its ability to accept electrons is represented by E_{LUMO}.[58,59] For developing the

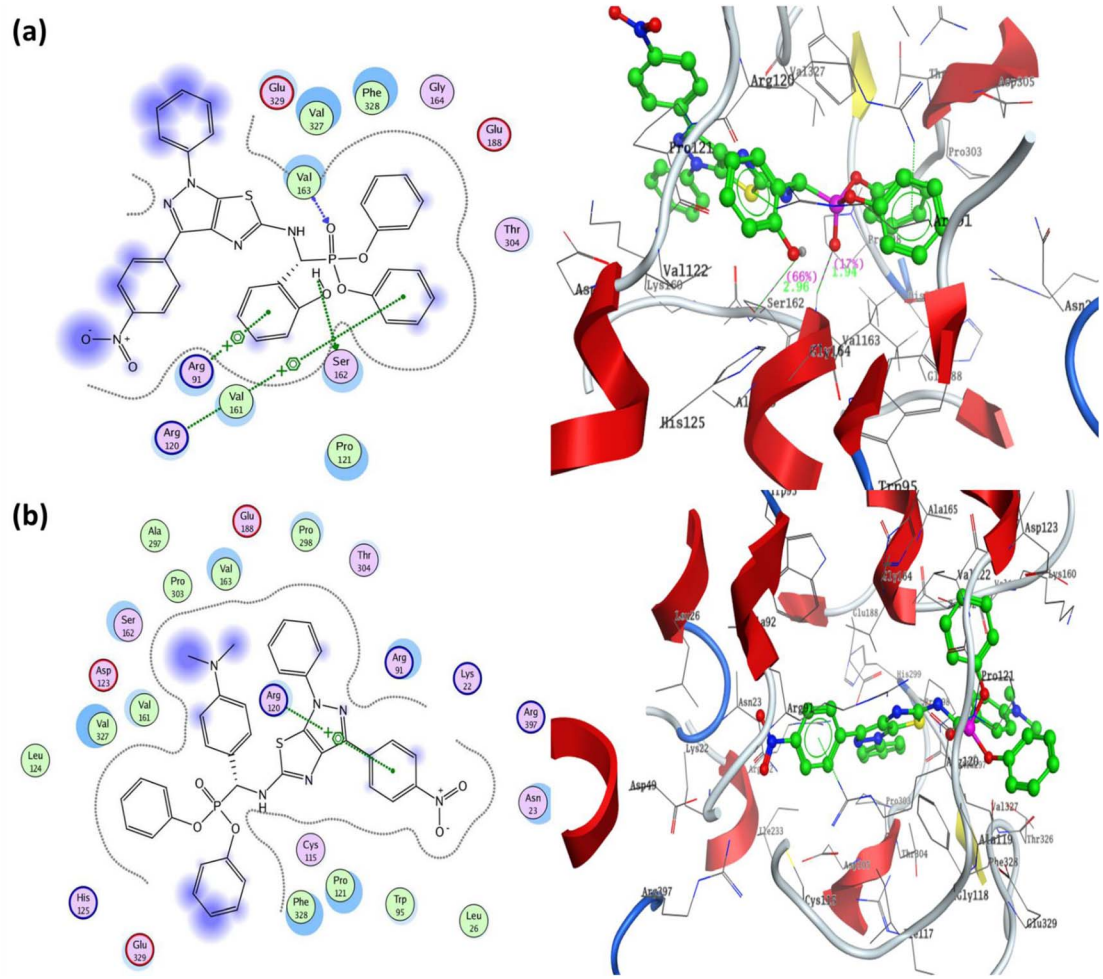

Fig. 6 Two-dimensional and three-dimensional structures of most active diphenyl α-aminophosphonate derivatives **5a** and **5b** inside the active site of Mur A (**PDB**: 1AUE) (a) **5a**/1AUE and (b) **5b**/1AUE.

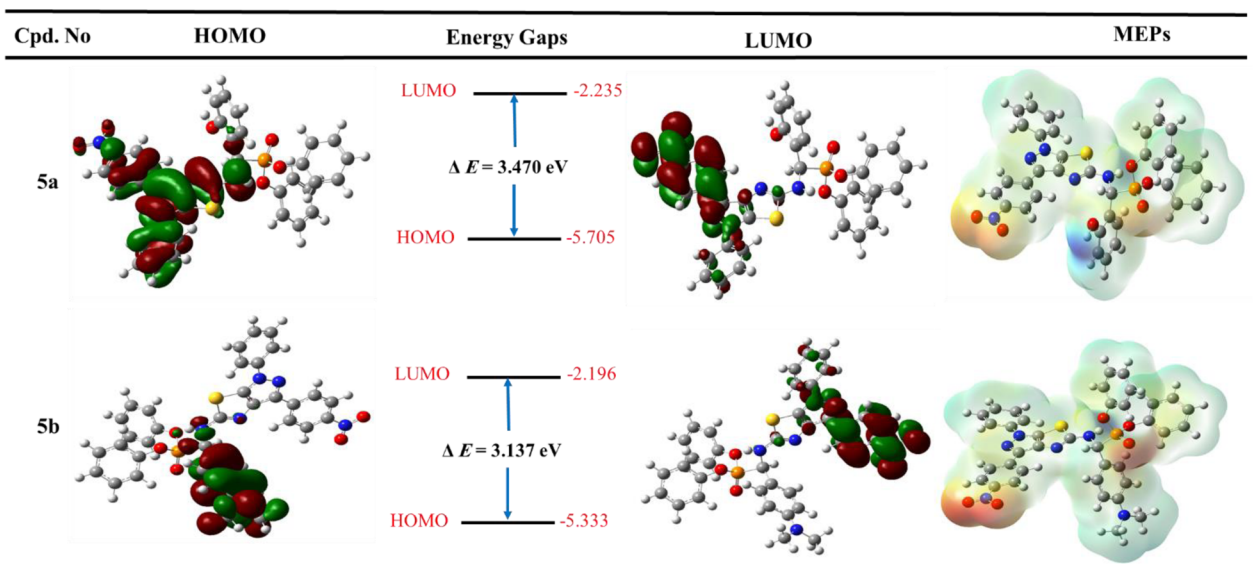

Fig. 7 Graph represented frontier molecular orbitals (FMOs) and their energies with molecular electrostatic potential (MEP maps) for the most active derivatives **5a** and **5b**.

concept of binding systems for drugs and receptors, the most active amino phosphonate derivative **5a** exhibited that the HOMO is mainly localized over pyrazolo[4,3-*d*]thiazole nucleus and methyl amine at C2 of pyrazolo[4,3-*d*]thiazole, while for amino phosphonate derivative **5b** distributed over benzylidene derivatives and the amino group of pyrazolo[4,3-*d*]thiazole moiety, indicating that these positions have high negative charges and therefore expected to be active sites and interacted with positively charged sites in the biological target. However, the LUMO orbitals for most active **5a** and **5b** were primarily concentrated on the pyrazole skeleton, N1-phenyl of pyrazole, and 4-nitrol phenyl at C3 of the pyrazolo[4,3-*d*]thiazole fragment slightly distributed over the thiazole core. The energies of HOMO, LUMO, and their band gaps for most active compounds were calculated, and are shown in Fig. 7. Moreover, the results exhibited that most active phosphonate derivatives **5a** and **5b** had energy band gaps of 3.470 and 3.137 eV.

Furthermore, the two phenyl groups of diphenyl phosphonates do not include both HOMOs and LUMOs. It suggested that these hydrophobic groups regulate the properties of physicochemical compounds. In addition, the HOMO and LUMO orbitals for fosfomycin (positive control) have dispersed over all structures, except the methyl group at the ethylene oxide ring that does not cove in the LUMO orbital (all figures in complete size are represented in the ESI† file).

To determine the charge distributed over the most active two diphenyl α-aminophosphonates **5a** and **5b**, the molecular electrostatic potential maps were generated and represented in Fig. 7. In addition, MEP maps explained the electrostatic interaction between the designed derivative and biological targets and the orientation of drug candidates in terms of their activity.[60,61] The negative positions on the molecules showed the oxygen of nitro group, oxygen of phosphonate, and nitrogen of pyrazole and thiazole fragments and represented as red color. Furthermore, the positive charge is represented by blue color and displayed on the NH group at C-2 of pyrazolo[4,3-*d*]thiazole derivatives and hydrogen of the hydroxyl group at **5a**. In addition, the neutral charge is distributed at all aryl groups and appears as green color. Finally, the quantum chemical study supports the binding mode obtained from the previous docking study.

3. Conclusion

In summary, a new series of α-aminophosphonates derivatives containing a pyrazolo[4,3-*d*]thiazole pharmacophore have been synthesized and fully characterized by $^{1}H/^{13}C$ NMR, IR, and mass spectroscopy, as well as elemental analysis. The newly synthesized derivatives were assessed *in vitro* for antimicrobial evaluation as evidence of the concept of designing new antimicrobial agents containing new pharmacophore moieties. A panel of MDR clinical isolates, including Gram +ve, Gram −ve bacteria, and fungi, were selected representing the most common UTI microorganisms. All the synthesized derivatives showed promising *in vitro* antimicrobial activity, with compounds **5a** and **5b** as the most potent microbicidal compounds, as represented by the ZOIs, MICs, MBCs and MFCs compared with fosfomycin and fluconazole in addition to the time-kill assay. Moreover, the most active derivatives **5a** and **5b** showed synergistic activity upon their combination with fosfomycin and fluconazole, except in case of **5b**, which showed partial synergistic activity when combined with fluconazole against the *Candida* isolates. In addition, it has been shown that the phosphonate compounds **5a** and **5b** act by disrupting the OM integrity of the bacterial cell walls as evidenced by both SEM analysis and EtBr accumulation assay. In addition, both **5a** and **5b** showed non-cytotoxicity against two normal cell lines, indicating their safety margin to the normal cells. Furthermore, these derivatives exhibited a potent inhibitory activity against the *E. coli* MurA enzyme compared with fosfomycin. The gamma sterilization of both compounds displayed a potent eradication effect on the active compounds' microbial load at 7.0 kGy without affecting the physicochemical properties of the antimicrobial agents. Finally, the molecular docking simulation of the promising derivatives **5a** and **5b** revealed binding energies $S = -23.46$ and -20.11 kcal mol^{-1} with good binding with specified receptor target compared with the fosfomycin $S = -10.89$ kcal mol^{-1}, with different types of interactions inside the active site of MUR A (**PDB**: 1UAE). In addition, the FMOs, including HOMO, LUMO, and energy band gap, as well as the graph of MEP maps displayed the electronic distribution over the molecules identifying positive and negative regions that interact with the biological target. In conclusion, the designed phosphonate moiety could be a potential non-cytotoxic antimicrobial agent in treating UTIs as MurA inhibitors.

4. Experimental section

4.1. Materials and instrumentation

All reagents of analytical grade were purchased from Sigma-Aldrich and used without further purification. All melting points were measured using a Gallenkamp melting point apparatus without corrections. The infrared spectra were recorded using a PerkinElmer FTIR 1430 spectrophotometer by the KBr disk technique. The ^{1}H NMR spectra were recorded using a Bruker AC spectrometer (500 MHz) at 25 °C in DMSO-d_6 with TMS as an internal standard, and chemical shifts are reported in ppm as δ values and ^{13}C NMR at 126 MHz. Mass spectra were recorded using a Finnigan MAT 8222 EX mass spectrometer at 70 eV. The elemental analyzer was performed at Microanalytical center at Cairo University and the values found to be within ±0.4% of the theoretical ones unless otherwise indicated. The reaction progress was monitored by thin-layer chromatography (TLC) using benzene/acetone (3/1 by volume) as eluent.

4.2. Chemistry

4.2.1. Synthesis of 3-(4-nitrophenyl)-1-phenyl-1*H*-pyrazolo[4,3-*d*]thiazol-5-amine (2). A solution of bromine (1.28 mL) dissolved in glacial acetic acid (5 mL) was added dropwise to a cooled mixture of 3-(4-nitrophenyl)-1-phenyl-1*H*-pyrazol-5-amine (**1**) (2.24 g, 8 mmol) and KSCN (6.4 g, 6.4 mmol) in glacial acetic acid (16 mL). After the addition of bromine, the solution was stirred at 0 °C for 2 h and at room temperature for

10 h. It was allowed to stand overnight, during which period an orange precipitate settled at the bottom, and water (6 mL) was added, heated to 85 °C and filtered hot. The residue was treated with glacial acetic acid (20 mL), heated again to 85 °C and filtered hot. The filtrate was cooled and neutralized with an ammonia solution to pH 6.0. A dark orange precipitate was crystallized from benzene/acetone of 1 : 1 to give compound **2**.

Yield: 76%; M.p.: over 360 °C; IR ν/max (cm^{-1}): 3357 (NH_2), 3095 (CH–Ar), 2966 (CH–aliph), 1565 (C═N), 682 (C–S); ^{1}H NMR (500 MHz, DMSO-d_6) δ/ppm 8.56 (dd, J = 8.2, 1.4 Hz, 1H, Ar–H), 8.25 (t, J = 9.0 Hz, 1H, Ar–H), 7.88 (t, J = 10.5 Hz, 1H, Ar–H), 7.68 (d, J = 10.5 Hz, 1H, Ar–H), 7.63–7.61 (m, 1H, Ar–H), 7.59 (d, J = 2.5 Hz, 1H, Ar–H), 7.58 (t, J = 2.5 Hz, 1H, Ar–H), 7.55 (d, J = 3.0 Hz, 1H, Ar–H), 7.53 (d, J = 3.5 Hz, 1H, Ar–H), 7.41 (s, 2H, NH_2 exchangeable with D_2O); ^{13}C NMR (126 MHz, DMSO-d_6) δ/ppm 158.28 (C–NH_2), 148.96 (C═N), 143.01, 140.73, 135.82, 130.97, 130.33, 130.24, 129.67, 129.48, 129.17, 127.59, 127.42, 127.26, 117.44, 116.38 (Ar–Cs); MS (EI) m/z: calcd for $C_{16}H_{11}N_5O_2S$ [M^+], 337.06; found, 337.75; Anal. Calcd. for $C_{16}H_{11}N_5O_2S$ (337.063): C, 56.96; H, 3.29; N, 20.76; found: C, 56.75; H, 3.42; N, 20.58.

4.2.2. Synthesis of α-amino phosphonate derivatives. To a stirred solution of 3-(4-nitrophenyl)-1-phenyl-1*H*-pyrazolo[4,3-*d*]thiazol-5-amine (**2**) (0.001 mol, 0.337 g) in dry dichloromethane CH_2Cl_2 (5 mL), triphenyl phosphite and/or triethyl phosphite (0.01 mol), appropriate aldehyde (0.001 mol) and anhydrous lithium perchlorate $LiClO_4$ (10 mol%) were added. The reaction mixture was stirred at room temperature (48 h) until completion of the reaction, as indicated by TLC. Then, CH_2Cl_2 was evaporated, and the α-amino phosphonates were precipitated using methanol. The precipitate was filtered off and new α-aminophosphonates were obtained in excellent yields.

4.2.3. Diethyl((4-chlorophenyl)((3-(4-nitrophenyl)-1-phenyl-1*H*-pyrazolo[4,3-*d*]thiazol-5-yl)amino)methyl) phosphonate (3). Yield: 82%; M.p. = 298–300 °C; IR: ν/cm^{-1}: IR: ν/cm^{-1}: 3345 (NH), 3059 (CH–Arom.), 2998 (CH–Aliph.), 1555 (C═N), 1252 (P═O); 1061 (P–O–C), 769 (P–CH); ^{1}H NMR (500 MHz, DMSO-d_6) δ/ppm 9.72 (s, 1H, NH exchangeable with D_2O), 8.13 (d, 4H, Ar–H), 7.83 (d, 2H, Ar–H), 7.64 (s, 1H, CH-methane), 7.44 (d, 4H, Ar–H), 6.96 (t, 3H, Ar–H), 3.85 (q, 4H, 2O − CH_2CH_3), 1.05 (t, 6H, 2O − CH_2CH_3); ^{13}C NMR (126 MHz, DMSO-d_6) δ/ppm 145.52, 144.19 (2C = N), 138.65, 137.16, 135.85, 132.21, 130.28, 130.07, 128.92, 128.46, 125.39, 122.55, 120.27, 119.74, 119.37, 117.43, 112.53, 108.90 (Ar–Cs), 66.80 (2O − CH_2CH_3), 59.58 (CH), 12.23 (2O − CH_2CH_3); MS (EI) m/z: calcd for $C_{27}H_{25}ClN_5O_5PS$ [M^+], 598.01; found, 598.56; Anal. Calcd. for $C_{27}H_{25}ClN_5O_5PS$ (702.73): C, 54.23; H, 4.21; N, 11.71; found: C, 54.34; H, 4.19; N, 11.83.

4.2.4. Diethyl((4-(dimethylamino)phenyl)((3-(4-nitrophenyl)-1-phenyl-1*H*-pyrazolo[4,3-*d*]thiazol-5-yl)amino)methyl) phosphonate (4). Yield: 77%; M.p. = 352–354 °C; IR: ν/cm^{-1}: IR: ν/cm^{-1}: 3378 (NH), 3067 (CH–Arom.), 2954 (CH–Aliph.), 1568 (C═N), 1277 (P═O); 1095 (P–O–C), 776 (P–CH); ^{1}H NMR (500 MHz, DMSO-d_6) δ/ppm 9.53 (s, 1H, NH exchangeable with D_2O), 8.21 (d, J = 8.5 Hz, 2H, Ar–H), 8.07 (d, J = 9.0 Hz, 1H, Ar–H), 7.57 (d, J = 9.0 Hz, 3H, Ar–H), 7.53 (d, J = 6.5 Hz, 1H, Ar–H), 7.45 (t, J = 7.75 Hz, 3H, Ar–H), 6.90 (s, 1H, CH-methane), 6.66 (d, J = 9.0 Hz, 3H, Ar–H), 3.85 (q, J = 6.5 Hz, 4H, 2O − CH_2CH_3), 2.91 (s, 6H, $2CH_3$), 1.19 (t, J = 7.0 Hz, 3H, O − CH_2CH_3), 1.13 (t, J = 7.0 Hz, 3H, O − CH_2CH_3); ^{13}C NMR (126 MHz, DMSO-d_6) δ/ppm 146.41, 143.75 (2C = N), 139.31, 137.87, 133.88, 133.11, 130.64, 129.18, 129.00, 128.57, 124.81, 122.97, 122.73, 121.94, 119.98, 119.71 (Ar–Cs), 66.81 (2O − CH_2CH_3), 64.00 (CH), 35.33 ($2CH_3$), 22.05 (2O − CH_2CH_3); MS (EI) m/z: calcd for $C_{29}H_{31}N_6O_5PS$ [M^+], 606.63; found, 606.98; Anal. Calcd. for $C_{29}H_{31}N_6O_5PS$ (606.638): C, 57.42; H, 5.15; N, 13.85; found: C, 57.55; H, 5.09; N, 13.76.

4.2.5. Diphenyl((2-hydroxyphenyl)((3-(4-nitrophenyl)-1-phenyl-1*H*-pyrazolo[4,3-*d*]thiazol-5-yl)amino)methyl) phosphonate (5a). Yield: 80%; M.p. = 210–212 °C; IR: ν/cm^{-1}: IR (KBr, ν, cm^{-1}): 3366 (NH), 3091 (CH–Arom.), 2997 (CH–Aliph.), 1563 (C═N), 1251 (P═O); 1077 (P–O–C), 778 (P–CH); ^{1}H NMR (500 MHz, DMSO-d_6) δ/ppm 9.98 (s, 1H, OH exchangeable with D_2O), 9.67 (s, 1H, NH exchangeable with D_2O), 8.15 (d, J = 7.5 Hz, 2H, Ar–H), 8.03 (d, J = 8.5 Hz, 2H, Ar–H), 7.48 (d, J = 7.0 Hz, 3H, Ar–H), 7.23 (d, J = 8.0 Hz, 3H, Ar–H), 7.16 (d, J = 8.0 Hz, 2H, Ar–H), 7.10 (t, J = 8.0 Hz, 6H, Ar–H), 6.99 (t, J = 7.5 Hz, 4H, Ar–H), 6.62 (t, J = 8.25 Hz, 1H, Ar–H), 5.97 (s, 1H, CH-methane); ^{13}C NMR (126 MHz, DMSO-d_6) δ/ppm 149.86 (C–OH), 148.61, 147.16 (2C = N), 140.60, 139.50, 134.76, 132.87, 130.98, 130.12, 129.88, 129.54, 129.38, 129.07, 129.00, 128.86, 125.77, 120.59, 118.34, 115.05 (Ar–Cs), 66.81 (CH); MS (EI) m/z: calcd for $C_{35}H_{26}N_5O_6PS$ [M^+], 675.65; found, 675.80; Anal. Calcd. for $C_{35}H_{26}N_5O_6PS$ (675.65): C, 62.22; H, 3.88; N, 10.37; found: C, 62.45; H, 3.64; N, 10.12.

4.2.6. Diphenyl((4-(dimethylamino)phenyl)((3-(4-nitrophenyl)-1-phenyl-1*H*-pyrazolo[4,3-*d*]thiazol-5-yl)amino)methyl) phosphonate (5b). Yield: 79%; M.p. = 190–192 °C; IR: ν/cm^{-1}: 3324 (NH), 3059 (CH–Arom.), 2988 (CH–Aliph.), 1565 (C═N), 1237 (P═O); 1067 (P–O–C), 779 (P–CH); ^{1}H NMR (500 MHz, DMSO-d_6) δ/ppm 9.52 (s, 1H, NH exchangeable with D_2O), 8.16 (d, J = 8.5 Hz, 2H, Ar–H), 8.06 (d, J = 8.5 Hz, 2H, Ar–H), 7.58 (d, J = 7.5 Hz, 3H, Ar–H), 7.52 (d, J = 7.5 Hz, 1H, Ar–H), 7.41 (t, J = 8.5 Hz, 3H, Ar–H), 7.27 (d, J = 6.5 Hz, 3H, Ar–H), 7.13 (t, J = 6.5 Hz, 3H, Ar–H), 6.99 (t, J = 6.75 Hz, 2H, Ar–H), 6.86 (s, 1H, CH-methane), 6.72 (d, J = 7.0 Hz, 3H, Ar–H), 6.65 (t, J = 7.0 Hz, 1H, Ar–H), 2.91 (s, 6H, $2CH_3$); ^{13}C NMR (126 MHz, DMSO-d_6) δ/ppm 146.41, 143.75 (2C = N), 139.31, 137.87, 133.88, 133.11, 130.64, 129.18, 129.00, 128.57, 124.81, 122.97, 122.73, 121.94, 119.98, 119.71 (Ar–Cs), 64.00 (CH), 35.33 ($2CH_3$); MS (EI) m/z: calcd for $C_{37}H_{31}N_6O_5PS$ [M] $^+$, 702.73; found, 702.99; Anal. Calcd. for $C_{37}H_{31}N_6O_5PS$ (702.73): C, 63.24; H, 4.45; N, 11.96; found: C, 63.09; H, 4.74; N, 11.71.

4.2.7. Diphenyl(((3-(4-nitrophenyl)-1-phenyl-1*H*-pyrazolo[4,3-*d*]thiazol-5-yl)amino)(thiophen-2-yl)methyl)phosphonate (6a). Yield: 75.7%; M.p. = 162–163 °C; IR: ν/cm^{-1}; 3320 (NH), 3058 (CH–Arom.), 2998 (CH–Aliph.), 1556 (C═N), 1255 (P═O); 1076 (P–O–C), 776 (P–CH);^{1}H NMR (500 MHz, DMSO-d_6) δ/ppm 9.72 (s, 1H, NH exchangeable with D_2O), 8.17 (d, J = 7.5 Hz, 2H, Ar–H), 8.05 (d, J = 6.0 Hz, 2H, Ar–H), 7.86 (t, J = 7.75 Hz, 1H, Ar–H), 7.70 (d, J = 8.0 Hz, 2H, Ar–H), 7.50 (d, J = 7.5 Hz, 2H, Ar–H), 7.40 (t, J = 7.75 Hz, 3H, Ar–H), 7.27 (t, d, J = 7.5 Hz, 3H, Ar–H), 7.12 (d, J = 7.5 Hz, 2H, Ar–H), 7.00 (t, d, J = 7.75 Hz, 3H, Ar–H), 6.64 (d, J = 7.5 Hz, 2H, Ar–H), 5.99 (s, 1H, CH-methane); ^{13}C NMR (126 MHz, DMSO-d_6) δ/ppm 149.35, 147.92 (2C = N),

146.50, 144.83, 140.62, 138.62, 136.99, 134.20, 129.49, 128.88, 128.03, 121.95, 121.18, 120.65, 114.41, 66.84 (CH); MS (EI) *m*/*z*: calcd for $C_{33}H_{24}N_5O_5PS_2$ [M^+], 665.67; found, 665.74; Anal. Calcd. for $C_{33}H_{24}N_5O_5PS_2$ (665.67): C, 59.54; H, 3.63; N, 10.52; found: C, 59.49; H, 3.71; N, 10.52.

4.2.8. Diphenyl(((3-(4-nitrophenyl)-1-phenyl-1*H*-pyrazolo[4,3-*d*]thiazol-5-yl)amino)(1*H*-pyrrol-2-yl)methyl)phosphonate (6b). Yield: 81%; M.p. = 112–113 °C; IR: ν/cm^{-1}: 3377 (NH), 3076 (CH–Arom.), 2978 (CH–Aliph.), 1644 (C=N), 1264 (P=O); 1069 (P–O–C), 776 (P–CH); ^{1}H NMR (500 MHz, DMSO-d_6) δ/ppm 9.29 (s, 1H, NH exchangeable with D_2O), 7.42 (t, J = 7.75 Hz, 1H, Ar–H), 7.33 (s, 1H, NH exchangeable with D_2O), 7.28 (d, J = 8.5 Hz, 2H, Ar–H), 7.25 (d, J = 8.0 Hz, 2H, Ar–H), 7.20 (t, J = 7.0 Hz, 3H, Ar–H), 7.13 (t, J = 8.25 Hz, 6H, Ar–H), 7.08 (d, J = 7.5 Hz, 2H, Ar–H), 7.02 (d, J = 8.0 Hz, 2H, Ar–H), 6.99 (d, J = 9.5 Hz, 2H, Ar–H), 6.64 (d, J = 7.5 Hz, 2H, Ar–H), 6.00 (s, 1H, CH-methane); ^{13}C NMR (126 MHz, DMSO-d_6) δ/ppm 149.86, 148.61 (2C = N), 147.16, 140.60, 139.50, 134.76, 132.87, 131.92, 131.51, 130.98, 130.12, 129.88, 129.54, 129.44, 129.38, 129.07, 129.00, 128.86, 125.77, 120.59, 118.34, 115.05, 66.81 (CH); MS (EI) *m*/*z*: calcd for $C_{33}H_{25}N_6O_5PS$ [M^+], 648.63; found, 648.73; Anal. Calcd. for $C_{33}H_{25}N_6O_5PS$ (648.63): C, 61.11; H, 3.89; N, 12.96; found: C, 61.25; H, 3.91; N, 12.86.

4.3. Biological evaluation

4.3.1. Microorganisms, constructs, media and chemicals. A panel of multidrug-resistant bacterial isolates were identified as Gram-positive bacteria (*Enterococcus faecalis*$_{KA247}$ and *Staphylococcus aureus*$_{KA112}$), Gram-negative bacteria (*Escherichia coli*$_{KA780}$ and *Proteus mirabilis*$_{KA320}$) as well as two fungal isolates identified as *Candida albicans*$_{KA205}$ and *Candida tropicalis* $_{KA205}$. The microbes were isolated from clinical samples from patients admitted with complicated urinary tract infections (cUTIs), at Central Laboratories, El-Kasr El-Aini Hospital, Cairo University, Cairo, Egypt. They were identified as multi-drug resistant isolates, *i.e.*, resistant to at least one antibiotic in three or more antimicrobial agents. In addition, a standard *E. coli* strain harboring the pSYC plasmid encoding AcrB (Kam3-AcrB) was used for the EtBr accumulation assay.

4.3.2. Antimicrobial screening. The preliminary *in vitro* antimicrobial activity of all synthesized compounds was screened against two broad-spectrum antibiotics (fosfomycin and fluconazole) used as positive controls, while DMSO was used as a negative control in this study. The agar well-diffusion method determined the antimicrobial activity in terms of zones of inhibition's diameters in millimeter according to the guidelines by Clinical Laboratory Standards Institute.[62,63] The microbial suspensions were prepared in Tryptic Soya and Sabouraud broths from test organisms sub-cultured on Tryptic Soya agar and Sabouraud agar plates. The experiments were carried out in triplicates.

4.3.3. MICs, MBCs, and MFCs. For further investigation, the antimicrobial activity of the synthesized phosphonates was screened against the tested MDR microbes *via* a broth microdilution method on 96-well polystyrene flatbottom microtiter plates (Sarstedt, Germany) according to the CLSI[62,63] guidelines. The 24 h culture of the tested isolates was standardized to 0.5 McFarland units at 625 nm. The stock solutions of the synthesized compounds were prepared in DMSO followed by 2-fold serial dilution to give a concentration ranging from 0.06 μg mL^{-1} to 256 μg mL^{-1}. Each compound-containing well and the antibiotics were inoculated with 1×10^8 CFU mL^{-1} and 1×10^6 CFU mL^{-1} for bacterial and fungal isolates, respectively. Each plate included the positive control (the microorganism without the antimicrobial) and the negative control (medium only). MIC was recorded as the lowest concentration of the compound that did not result in an absorbance at 595 nm that was higher than its respective control with the compound after 24 h of incubation at 37 °C. After 24 h incubation, a spotting assay was performed in order to determine the MBC and MFC. The plates of tryptic soya agar and Sabouraud dextrose agar were prepared and inoculated with 5 μL of the content of each microtiter pit. Plates were then incubated under the appropriate condition for CFU counting. MBC and MFC were recorded as the lowest concentration that did not result in an eye-observable culture in the solid medium after incubation. Each assay was also performed in triplicates.

4.3.4. Effect of phosphonates on time-kill curves. The time-kill experiments were carried out according to the previous studies,[64] with minor modifications. The time-kill study of active phosphonates and controls at 1/2MIC and MIC was performed in 50 mL volume conical flasks containing 20 mL of each isolate in the log phase growth (1×10^5 CFU mL^{-1} for bacteria and 1×10^4 CFU mL^{-1} for fungi). Aliquots of one mL of the tested media were taken at time intervals of 0, 2, 4, 6, 8, 12, 18, and 24 h; and of 0, 2, 4, 6, 8, 18, 24 and 48 h for bacterial and fungal isolates, respectively. The organisms without treatment were used as controls. The cell counts at each time point was determined using the plate counts. Data were analyzed as killing curves by plotting $\log_{10}$CFU mL^{-1} *vs.* time (h), as described previously.

4.3.5. Synergistic effect of active phosphonates on other antibiotics. The synergistic effect of active phosphonate compounds *in vitro* in combination with fosfomycin and fluconazole against the tested clinical isolates was determined by a standard checkerboard assay[65,66] represented as the fractional inhibitory concentration index (ΣFICI), using the predetermined MICs of each compound. In brief, suspensions of bacteria and fungi were prepared in PBS equivalent to 0.5 McFarland followed by dilution in TSB to achieve the density of 1×10^5 and 1×10^4 CFU mL^{-1}, respectively. The MIC of each test compound in combination with each antibiotic studied was determined as the lowest concentration of each combination in which no visible growth was observed. The fractional inhibitory concentration index (ΣFICI) was calculated according to the following formula:

$$\Sigma\text{FICI} = (\text{MIC of drug A in combinstion/MIC of drug A}) + (\text{MIC of drug B in combination/MIC of drug B})$$

In which, drug A is the antibiotic and drug B is the target compound; FICI ≤ 0.5 (synergism); 0.5 < FICI > 1 (partial synergism); 1 ≤ FICI < 2 (indifference); FICI ≥ 2 (antagonism).

4.3.6. Scanning electron microscope. DMSO or active phosphonate compounds at their MICs were added to *E. coli* cultures immediately after inoculation. Cells were incubated for 24 h, collected and washed three times using a sterile PBS solution. Fixation, dehydration, mounting and coating were performed as described previously.[67] Imaging was carried out using a scanning electron microscope at a magnifying power of x7.00kx (ZEISS EVO LS, UK).

4.3.7. *In vitro* accumulation assay of ethidium bromide (EtBr). To further determine the effect of phosphonate compounds on the outer membrane (OM) integrity of *E. coli*, the permeability of EtBr which cannot penetrate an intact OM was analysed. The EtBr accumulation assay was performed according to previous studies[55,68] with some modifications. The *E. coli* Kam3-AcrB cells were grown to a mid-log phase in a TS broth and then collected by centrifugation (5000×*g* for 5 min. at 4 °C). The collected cells were resuspended two times in a PBS solution containing 10 mM Na_2HPO_4, 1.8 mM KH_2PO_4, 0.5 mM $MgCl_2$, 1 mM $CaCl_2$, 2.7 mM KCl, and 137 mM NaCl at pH 7.4 and diluted in PBS till reaching an approximate of 0.5 at OD_{600}. The cell suspension (150 μL) was incubated in a 96-well microtiter plate with a filter sterilized glucose to a final concentration of 25 mM, EtBr (2 mM), the phosphonate compounds at MIC of 0.06 μg mL^{-1} to 2 μg mL^{-1}, and PaβN (20 μg mL^{-1}). The relative fluorescence intensity was measured over 38 min using a fluorescence plate reader (PerkinElmer Enspire 300®2300, USA). The emission and excitation wavelengths were 520 and 600 nm, respectively.

4.3.8. Cell culture. The cytotoxicity activity of the two most active compounds (**5a** and **5b**) was determined *in vitro* against two normal non-cancerous cell lines (**BNL**: mouse normal liver cell line and **Vero**: green monkey kidney cell line). Both cell lines were obtained from Nawah Scientific Inc. (Mokatam, Cairo, Egypt). DMEM media were supplemented with 100 mg mL^{-1} streptomycin, 100 units per mL penicillin, and 10% heat-inactivated fetal bovine serum in a humidified 5% (v/v) CO_2 atmosphere at 37 °C.

4.3.9. Cytotoxicity assay. A colorimetric SulphoRhodamine-B (SRB) assay was used to assess the cell viability. In brief, aliquots of 100 μL cell suspension (5×10^3 cells) were seeded in 96-well plates followed by incubation in complete media for 24 h. Cells were treated with another aliquot of 100 μL of media containing the tested derivatives and the control drug (Doxorubicin) at various concentrations (0.01, 0.1, 1.10 and 100 μM). After drug exposure, the treated cells were fixed by replacing media with 150 μL 10% triacetic acid (TCA) and then re-incubated at 4 °C for 1 h. The TCA solution was removed and the cells were washed 5 times with distilled water. Aliquots of 70 μL SRB solution (0.4% w/v) were added and incubated in a dark place at room temperature for 10 min. Plates were washed 3 times with 1% acetic acid and left to air-dry overnight. Then, 150 μL of TRIS (10 mM) was added to dissolve the protein-bound SRB stain; the absorbance was measured at 540 nm using an Infinite F50 microplate reader (TECAN, Switzerland).

4.3.10. Inhibitory activity of phosphonates on MurA enzyme. MurA inhibition was determined by the colorimetric malachite green method upon measuring the concentration of orthophosphate released during the reaction.[69,70] In brief, 2.5 μL of each tested compound dissolved in DMSO at a concentration of 100 μM was added in duplicates to the reaction mixture (50 μL) containing 50 mM HEPES, pH 7.8, 0.005% Triton X-114, 200 μM UDP-GlcNAc, 100 μM PEP and 200 nM purified MurA diluted in 50 mM HEPES. The 50 μL time-dependent inhibition assays were also performed. The MurA was preincubated with a UDP-GlcNAc substrate and the target compounds at 37 °C for 10 min, followed by the addition of the second substrate PEP to give a mixture with a final concentration of 50 μL, as described above. In both experiments, after 15 min incubation at 37 °C, the reaction was stopped by adding Biomol® reagent (100 μL, Enzo Life Sciences Inc., NY, USA). The absorbance was measured at 650 nm after 5 min using a microplate reader. Fosfomycin was used as a reference in the MurA assay. The percentage of residual activity (RA) was calculated in comparison to negative controls containing 5% DMSO (v/v). The IC_{50} values, the concentration of the compound at which the RA was 50%, were determined by measuring the residual activities at different concentrations. The results were recorded as mean ± standard error.

4.3.11. Effect of gamma radiation on the microbial load of the active phosphonate compounds. Gamma radiation has been extensively used as an advantageous method for the sterilization of different pharmaceutical products.[71,72] The active phosphonate compounds were subjected to different irradiation doses (3.0, 5.0, 7.0, 10.0, 15.0, and 20.0 kGy) using a radioactive source of 60-Cobalt (^{60}Co) located in the National Center of Research and Radiation Technology (NCRRT), Egyptian Atomic Energy Authority, Egypt. The radiation dose at the time of the experiment was 0.9 kGy h^{-1}. They were all in powder form and were transferred into sterile Eppendorf tubes for the irradiation process. The changes in the physical and chemical properties of both non-irradiated and irradiated compounds were observed and detected using a UV-VIS spectrophotometer at 560 nm. After that, a microbiological sterility assay was performed. An aliquot of 0.05 g of each sample, either irradiated or non-irradiated, was added under aseptic conditions to test tubes containing 4.5 mL sterile saline. The test tubes were well-shaken and then 100 μL from each tube was transferred onto plates of Tryptic Soya agar and Sabouraud agar. Two plates were used for each dose. The plates were then incubated under ambient conditions, and then, the microbial count was recorded in CFU g^{-1}. The irradiated samples were used as controls in the assay.[73,74]

4.4. Molecular docking simulation

The molecular docking study for the most active diphenyl α-aminophosphonate derivatives **5a**, **5b** and fosfomycin (as positive control) was carried out inside the active site of UDP-*N*-acetylglucosamine enolpyruvyl transferase (MUR A, **PDB**: 1UAE). The 3D crystal structure has been retrieved from the protein data bank (**https://www.rcsb.org/structure/1uae**. Accessed on 21/3/2023),[57] where this protein is isolated from *E. coli* with resolution =1.80 Å and present in the complex

with a co-crystallized ligand uridine-diphosphate-*n*-acetylglucosamine (UD1). The docking simulation was performed using the Molecular Operating Environmental (MOE) software[75–77] version 10.2009. The validation process was performed using the triangle matcher placement, and London dG as rescoring 1 with refinement known as forcefield and retain thirty pose, as well as removing the duplication according to the reported method.[78] The validation process exhibited that the co-crystallized ligand showed binding energy $S = -17.69$ kcal mol^{-1} with RMSD = 1.53 Å, where the superimposition of the co-crystallized ligand (turquoise) and the re-docked co-crystallized (green) are described in the ESI† file. The co-crystallized ligand (UD1) exhibited five hydrogen bond sidechain acceptors with bond lengths as Arg91 (1.75 Å, 84%), ser162 (1.92 Å, 45%), Lys160 (1.74 Å, 62%), and Arg120 (1.97 Å with 51% and 2.07 Å with 23%). Moreover, the UD1 displayed two sidechain donors with residues Asp305 (1.90 Å, 35%) and Asp123 (1.73 Å, 24%) and three hydrogen bond backbone acceptor with residues Gly164 (1.99 Å, 43%), Val163 (1.84 Å, 63%), and Val327 (1.81 Å, 18%). The structure of the diphenyl α-aminophosphonate derivatives **5a**, **5b** and fosfomycin was built using ChemBioDraw 2014, and the structures were exported to MOE; then, the structures were subjected to protonated 3D, and energy was minimized using gradient 0.0001, as described previously.[79,80]

4.5. Quantum chemical studies

The quantum chemical studies, including frontier molecular orbital model (FMOs) and electrostatic potential, were calculated using density functional theory (DFT) in Gaussian 09W and visualized using Gaussian View 6.0. In addition, the molecules were optimized using hybrid functional B3LYP and basis set 6-31G(d), as described previously.[81–83]

Conflicts of interest

The authors declare no conflicts of interest.

References

1 A. Y. Alzahrani, Y. A. Ammar, M. Abu-Elghait, M. A. Salem, M. A. Assiri, T. E. Ali and A. Ragab, *Bioorg. Chem.*, 2022, **119**, 105571.
2 E. D. Naydenova, P. T. Todorov, P. I. Mateeva, R. N. Zamfirova, N. D. Pavlov and S. B. Todorov, *Amino Acids*, 2010, **39**, 1537–1543.
3 T. N. M. An, N. Van Cuong, N. M. Quang, T. V. Thanh and M. Alam, *ChemistrySelect*, 2020, **5**, 6339–6349.
4 S. Shaikh, P. Dhavan, G. Pavale, M. M. V Ramana and B. L. Jadhav, *Bioorg. Chem.*, 2020, **96**, 103589.
5 H. Patnala, H. S. Abbo, K. M. Potla, S. J. J. Titinchi and S. Chinnam, *Phosphorus, Sulfur Silicon Relat. Elem.*, 2019, **194**, 1035–1039.
6 B. Sujatha, S. Mohan, C. Subramanyam and K. P. Rao, *Phosphorus, Sulfur Silicon Relat. Elem.*, 2017, **192**, 1110–1113.
7 A. K. Bhattacharya, K. C. Rana, C. Pannecouque and E. De Clercq, *ChemMedChem*, 2012, **7**, 1601–1611.
8 M. A. Azzam, H. A. L. El-Boraey and I. E. T. El-Sayed, *Phosphorus, Sulfur Silicon Relat. Elem.*, 2020, **195**, 339–347.
9 R.-Z. Huang, C.-Y. Wang, J.-F. Li, G.-Y. Yao, Y.-M. Pan, M.-Y. Ye, H.-S. Wang and Y. Zhang, *RSC Adv.*, 2016, **6**, 62890–62906.
10 J. Che, X. Xu, Z. Tang, Y. Gu and D. Shi, *Bioorg. Med. Chem. Lett.*, 2016, **26**, 1310–1313.
11 Z. Jiang, J. Zhao, B. Gao, S. Chen, W. Qu, X. Mei, C. Rui, J. Ning and D. She, *Phosphorus, Sulfur Silicon Relat. Elem.*, 2013, **188**, 1026–1037.
12 H. Singh and A. K. Jain, *J. Appl. Polym. Sci.*, 2009, **111**, 1115–1143.
13 H. Ai, K. Xu, H. Liu, M. Chen and X. Zhang, *J. Appl. Polym. Sci.*, 2009, **113**, 541–546.
14 J. Canadell, B. J. Hunt, A. G. Cook, A. Mantecón and V. Cádiz, *Polym. Degrad. Stab.*, 2007, **92**, 1482–1490.
15 M. Salasi, T. Shahrabi, E. Roayaei and M. Aliofkhazraei, *Mater. Chem. Phys.*, 2007, **104**, 183–190.
16 K. Kavipriya, S. Rajendran, J. Sathiyabama and A. S. Prabha, *Eur. Chem. Bull.*, 2012, **1**, 366–374.
17 N. Moszner, F. Zeuner, U. K. Fischer and V. Rheinberger, *Macromol. Chem. Phys.*, 1999, **200**, 1062–1067.
18 I. Cabasso, J. Smid and S. K. Sahni, *J. Appl. Polym. Sci.*, 1990, **41**, 3025–3042.
19 L. H. Taboada, M. Guzmann, K. Neubecker and A. Göthlich, *US Pat.*, 12/520642, 2010.
20 M. Ordóñez, H. Rojas-Cabrera and C. Cativiela, *Tetrahedron*, 2009, **65**, 17–49.
21 C. S. Demmer, N. Krogsgaard-Larsen and L. Bunch, *Chem. Rev.*, 2011, **111**, 7981–8006.
22 H. Yu, H. Yang, E. Shi and W. Tang, *Med. Drug Discovery*, 2020, **8**, 100063.
23 F. Cambazard, *J. Eur. Acad. Dermatol. Venereol.*, 1998, **11**, S20–S27.
24 J. M. Rybak and K. Roberts, *Infect. Dis. Ther.*, 2015, **4**, 1–14.
25 K. Richardson, K. Cooper, M. S. Marriott, M. H. Tarbit, F. Troke and P. J. Whittle, *Rev. Infect. Dis.*, 1990, **12**, S267–S271.
26 K. Papangkorn, K. R. Truett, A. T. Vitale, C. Jhaveri, D. K. Scales, C. S. Foster, A. Montieth, J. W. Higuchi, B. Brar and W. I. Higuchi, *Curr. Eye Res.*, 2019, **44**, 185–193.
27 D. R. Budman, L. N. Igwemezie, S. Kaul, J. Behr, S. Lichtman, P. Schulman, V. Vinciguerra, S. L. Allen, J. Kolitz and K. Hock, *J. Clin. Oncol.*, 1994, **12**, 1902–1909.
28 S. Pol, M. Corouge and A. Vallet-Pichard, *Hepatic Med. Evid. Res.*, 2016, **8**, 21–26.
29 B. Litim, A. Djahoudi, S. Meliani and A. Boukhari, *Med. Chem. Res.*, 2022, **31**, 60–74.
30 G. Sravya, A. Balakrishna, G. V. Zyryanov, G. Mohan, C. S. Reddy and N. Bakthavatchala Reddy, *Phosphorus, Sulfur Silicon Relat. Elem.*, 2021, **196**, 353–381.
31 C. S. Transactions, *Chem. Sci. Trans.*, 2019, **8**, 359–367.
32 G. Gao, M.-N. Chen, L.-P. Mo and Z.-H. Zhang, *Phosphorus, Sulfur Silicon Relat. Elem.*, 2019, **194**, 528–532.
33 P. R. Varga and G. Keglevich, *Molecules*, 2021, **26**, 2511.

34 S. A. Ibrahim, E. A. Fayed, H. F. Rizk, S. E. Desouky and A. Ragab, *Bioorg. Chem.*, 2021, **116**, 105339.
35 G. S. Masaret, *ChemistrySelect*, 2021, **6**, 974–982.
36 A. R. Sayed, S. M. Gomha, F. M. Abdelrazek, M. S. Farghaly, S. A. Hassan and P. Metz, *BMC Chem.*, 2019, **13**, 116.
37 S. J. Takate, A. D. Shinde, B. K. Karale, H. Akolkar, L. Nawale, D. Sarkar and P. C. Mhaske, *Bioorg. Med. Chem. Lett.*, 2019, **29**, 1199–1202.
38 H. Barreteau, A. Kovač, A. Boniface, M. Sova, S. Gobec and D. Blanot, *FEMS Microbiol. Rev.*, 2008, **32**, 168–207.
39 M. Hrast, I. Sosič, R. Šink and S. Gobec, *Bioorg. Chem.*, 2014, **55**, 2–15.
40 A. Gautam, P. Rishi and R. Tewari, *Appl. Microbiol. Biotechnol.*, 2011, **92**, 211–225.
41 T. Van Cauwenbergh, E. Theys, D. Stroeykens, B. Croonenborghs, A. Gillet, A. DeMent, A. Van Schepdael and E. Haghedooren, *J. Pharm. Sci.*, 2022, **111**, 2011–2017.
42 E. A. Fayed, M. Mohsen, S. M. A. El-Gilil, D. S. Aboul-Magd and A. Ragab, *J. Mol. Struct.*, 2022, **1262**, 133028.
43 S. A. Ibrahim, H. F. Rizk, D. S. Aboul-Magd and A. Ragab, *Dyes Pigm.*, 2021, **193**, 109504.
44 A. Ragab, M. S. Abusaif, N. A. Gohar, D. S. Aboul-Magd, E. A. Fayed and Y. A. Ammar, *Bioorg. Chem.*, 2023, **131**, 106307.
45 S. A. Ibrahim, A. Ragab and H. A. El-Ghamry, *Appl. Organomet. Chem.*, 2022, **36**, 1–17.
46 H. F. Rizk, M. A. El-Borai, A. Ragab, S. A. Ibrahim and M. E. Sadek, *Polycyclic Aromat. Compd.*, 2023, **43**, 500–522.
47 A. S. Hassan, N. M. Morsy, W. M. Aboulthana and A. Ragab, *Drug Dev. Res.*, 2023, **84**, 3–24.
48 H. F. Rizk, M. A. El-Borai, A. Ragab and S. A. Ibrahim, *J. Iran. Chem. Soc.*, 2020, **17**, 2493–2505.
49 Y. A. Ammar, J. A. Micky, D. S. Aboul-Magd, S. M. A. Abd El-Hafez, S. A. Hessein, A. M. Ali and A. Ragab, *Chem. Biol. Drug Des.*, 2023, **101**(2), 245–270.
50 M. M. Abdelgalil, Y. A. Ammar, G. A. M. Elhag Ali, A. K. Ali and A. Ragab, *J. Mol. Struct.*, 2023, **1274**, 134443.
51 H. Mohammad, A. S. Mayhoub, M. Cushman and M. N. Seleem, *J. Antibiot.*, 2015, **68**, 259–266.
52 A. Ragab, M. S. Abusaif, D. S. Aboul-Magd, M. M. S. Wassel, G. A. M. Elhagali and Y. A. Ammar, *Drug Dev. Res.*, 2022, 1305–1330.
53 A. Ragab, S. A. Fouad, Y. A. Ammar, D. S. Aboul-Magd and M. S. Abusaif, *Antibiotics*, 2023, **12**(1), 128.
54 Y. A. Ammar, A. A. Farag, A. M. Ali, S. A. Hessein, A. A. Askar, E. A. Fayed, D. M. Elsisi and A. Ragab, *Bioorg. Chem.*, 2020, **99**, 103841.
55 W.-J. Lu, H.-J. Lin, T. K. Janganan, C.-Y. Li, W.-C. Chin, V. N. Bavro and H.-T. V. Lin, *Int. J. Mol. Sci.*, 2018, **19**(4), 1000.
56 T. J. Opperman, S. M. Kwasny, K. Hong-Suk, S. T. Nguyen, H. Chad, D. Sanjay, G. C. Walker, N. P. Peet, N. Hiroshi and T. L. Bowlin, *Antimicrob. Agents Chemother.*, 2014, **58**, 722–733.
57 **https://www.rcsb.org/structure/1t2w**, accessed on 20/7/2022.
58 A. A. Ali, H. Abd El-Wahab, M. S. Abusaif, A. Ragab, O. A. Abdel-Jaid, E. A. Eldeeb and Y. A. Ammar, *Pigm. Resin Technol.*, 2023, DOI: **10.1108/PRT-12-2022-0141**.
59 S. A. El-Kalyoubi, A. Ragab, O. A. Abu Ali, Y. A. Ammar, M. G. Seadawy, A. Ahmed and E. A. Fayed, *Pharmaceuticals*, 2022, **15**(3), 367.
60 R. Ayman, M. S. Abusaif, A. M. Radwan, A. M. Elmetwally and A. Ragab, *Eur. J. Med. Chem.*, 2023, **249**, 115138.
61 D. M. Elsisi, A. Ragab, A. A. Elhenawy, A. A. Farag, A. M. Ali and Y. A. Ammar, *J. Mol. Struct.*, 2022, **1247**, 131314.
62 R. Humphries, A. M. Bobenchik, J. A. Hindler and A. N. Schuetz, *J. Clin. Microbiol.*, 2021, **59**(12), e0021321.
63 B. D. Alexander, G. W. Procop, P. Dufresne, J. Fuller and M. A. Ghannoum, *Clin. Lab. Stand. Inst.*, 2017, **3**, M27-A3.
64 B. T. Tsuji, J. C. Yang, A. Forrest, P. A. Kelchlin and P. F. Smith, *J. Antimicrob. Chemother.*, 2008, **62**, 156–160.
65 H. Ali Mohamed, Y. A. Ammar, G. A. M. Elhagali, H. A. Eyada, D. S. Aboul-Magd and A. Ragab, *ACS Omega*, 2022, **7**, 4970–4990.
66 S. Kumar, V. Saini, I. K. Maurya, J. Sindhu, M. Kumari, R. Kataria and V. Kumar, *PLoS One*, 2018, **13**, e0196016.
67 A. G. Dale, J. Hinds, J. Mann, P. W. Taylor and S. Neidle, *Biochemistry*, 2012, **51**, 5860–5871.
68 A. R. Brown, K. A. Ettefagh, D. Todd, P. S. Cole, J. M. Egan, D. H. Foil, T. N. Graf, B. D. Schindler, G. W. Kaatz and N. B. Cech, *PLoS One*, 2015, **10**, e0124814.
69 A. Perdih, M. Hrast, H. Barreteau, S. Gobec, G. Wolber and T. Solmajer, *Bioorg. Med. Chem.*, 2014, **22**, 4124–4134.
70 B. Plackett, *Nature*, 2020, **586**, S50+.
71 S. Abdou and S. Ebraheem, *Egypt J. Radiat. Res. Appl.*, 2018, **31**, 137–142.
72 Ş. Çolak, *Evolution of Ionizing Radiation Research*, 2015, vol. 12, pp. 281–306.
73 S. H. M. Husseiny and F. A. Helimish, *World Appl. Sci. J.*, 2012, **19**, 847–855.
74 A. Özer, S. Turker, S. Çolak, M. Korkmaz, E. Kiliç and M. Özalp, *Interv. Med. Appl. Sci.*, 2013, **5**, 122–130.
75 H. Ali Mohamed, Y. A. Ammar, G. A. M. Elhagali, H. A. Eyada, D. S. Aboul-Magd and A. Ragab, *J. Mol. Struct.*, 2023, **1287**(5), 135671.
76 E. S. A. E. H. Khattab, A. Ragab, M. A. Abol-Ftouh and A. A. Elhenawy, *J. Biomol. Struct. Dyn.*, 2022, **40**, 1–19.
77 A. S. Hassan, N. M. Morsy, W. M. Aboulthana and A. Ragab, *RSC Adv.*, 2023, **13**, 9281–9303.
78 K. Rožman, S. Lešnik, B. Brus, M. Hrast, M. Sova, D. Patin, H. Barreteau, J. Konc, D. Janežič and S. Gobec, *Bioorg. Med. Chem. Lett.*, 2017, **27**, 944–949.
79 M. Eldeeb, E. F. Sanad, A. Ragab, Y. A. Ammar, K. Mahmoud, M. M. Ali and N. M. Hamdy, *Biomedicines*, 2022, **10**, 722.
80 A. Ragab, Y. A. Ammar, A. Ezzat, A. M. Mahmoud, M. Basseem, I. Mohamed, A. S. El-tabl and R. S. Farag, *Comput. Biol. Med.*, 2022, **145**, 105473.
81 K. E. Saadon, N. M. H. Taha, N. A. Mahmoud, G. A. M. Elhagali and A. Ragab, *J. Iran. Chem. Soc.*, 2022, **19**, 3899–3917.
82 R. Ayman, A. M. Radwan, A. M. Elmetwally, Y. A. Ammar and A. Ragab, *Arch. Pharm.*, 2023, **365**, 2200395.
83 M. S. Abusaif, A. M. Hyba, Y. A. Ammar, M. A. Salem, D. M. Elsisi and A. Ragab, *J. Taiwan Inst. Chem. Eng.*, 2023, **153**, 105207.